Figure S1

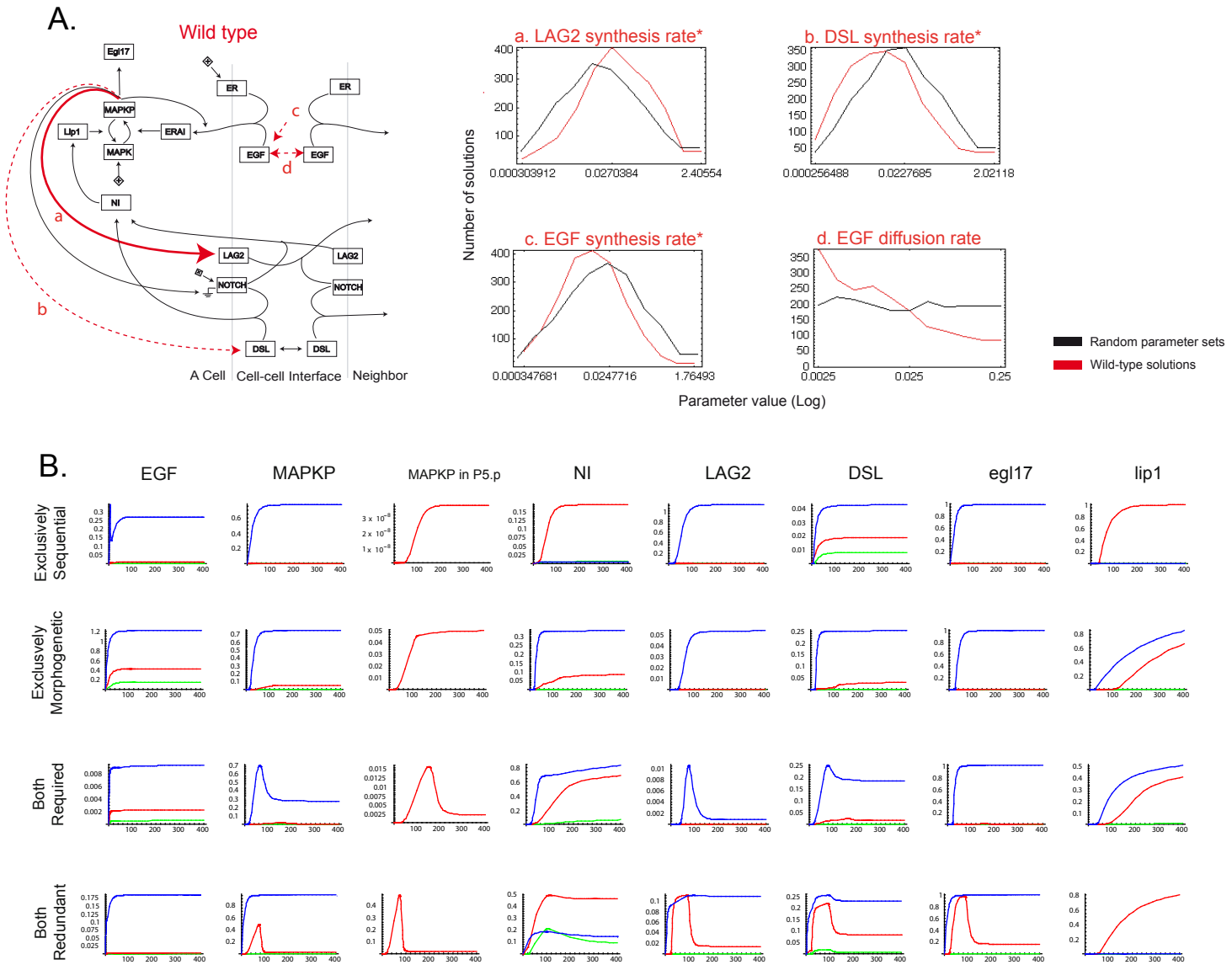

Figure S1

Figure S2

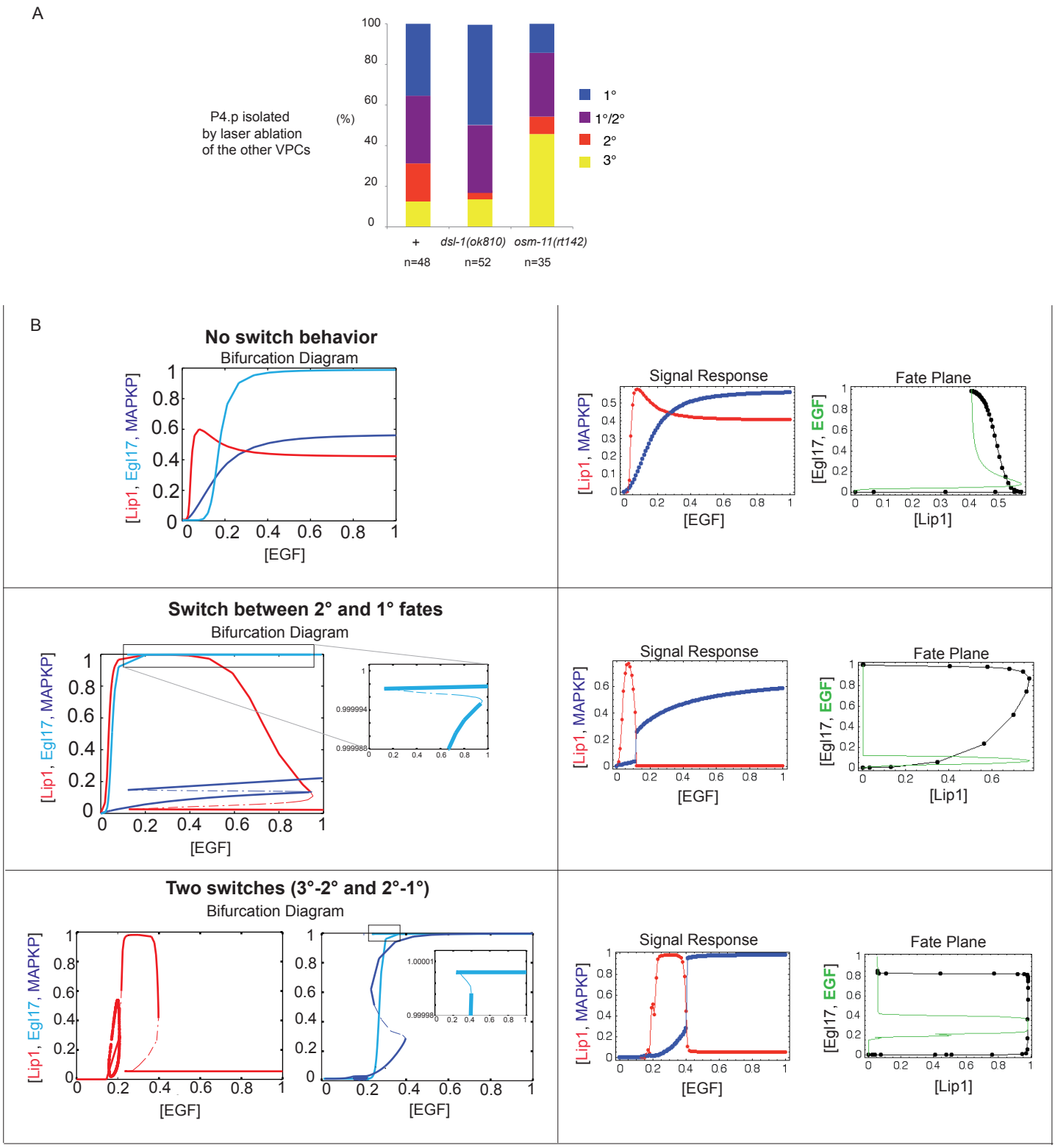

Figure S2

Figure S3

A

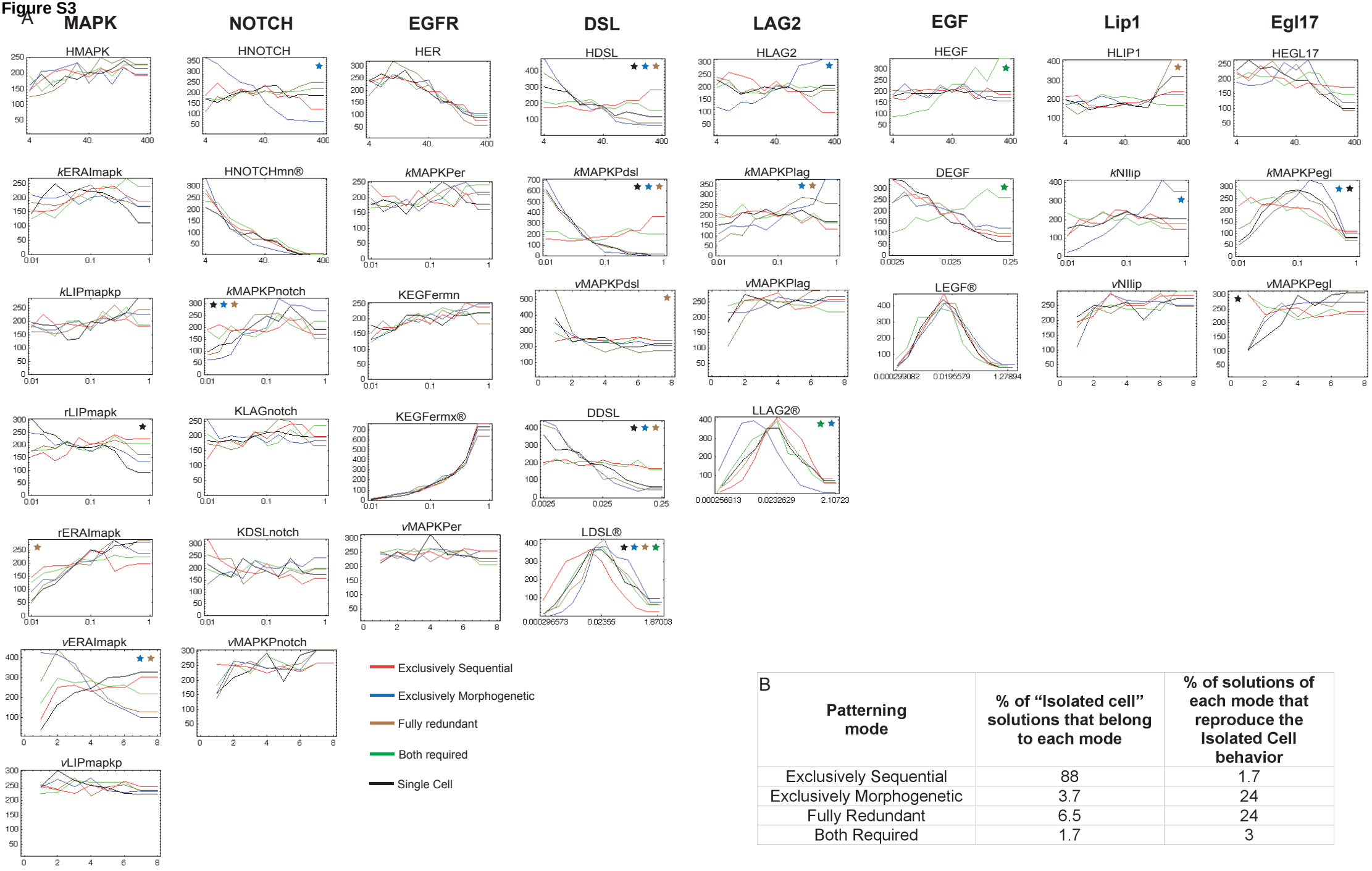

B

Patterning mode	% of "Isolated cell" solutions that belong to each mode	% of solutions of each mode that reproduce the Isolated Cell behavior
Exclusively Sequential	88	1.7
Exclusively Morphogenetic	3.7	24
Fully Redundant	6.5	24
Both Required	1.7	3

Figure S3

Figure S4

A

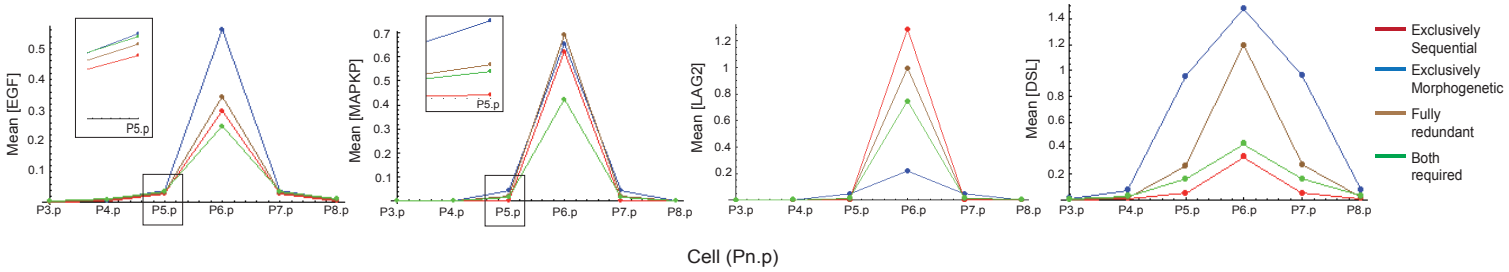

Protein	Mean expression ratio in P6.p/P5.p			
	Exclusively Sequential	Exclusively Morphogenetic	Fully Redundant	Both Required
EGF	41	37	34	19
MAPKP	183.417	10	1.258	168
LAG2	$7x10^{18}$	28	$2x10^{10}$	694.186
DSL	6.8	1.5	58.6	8.1

B

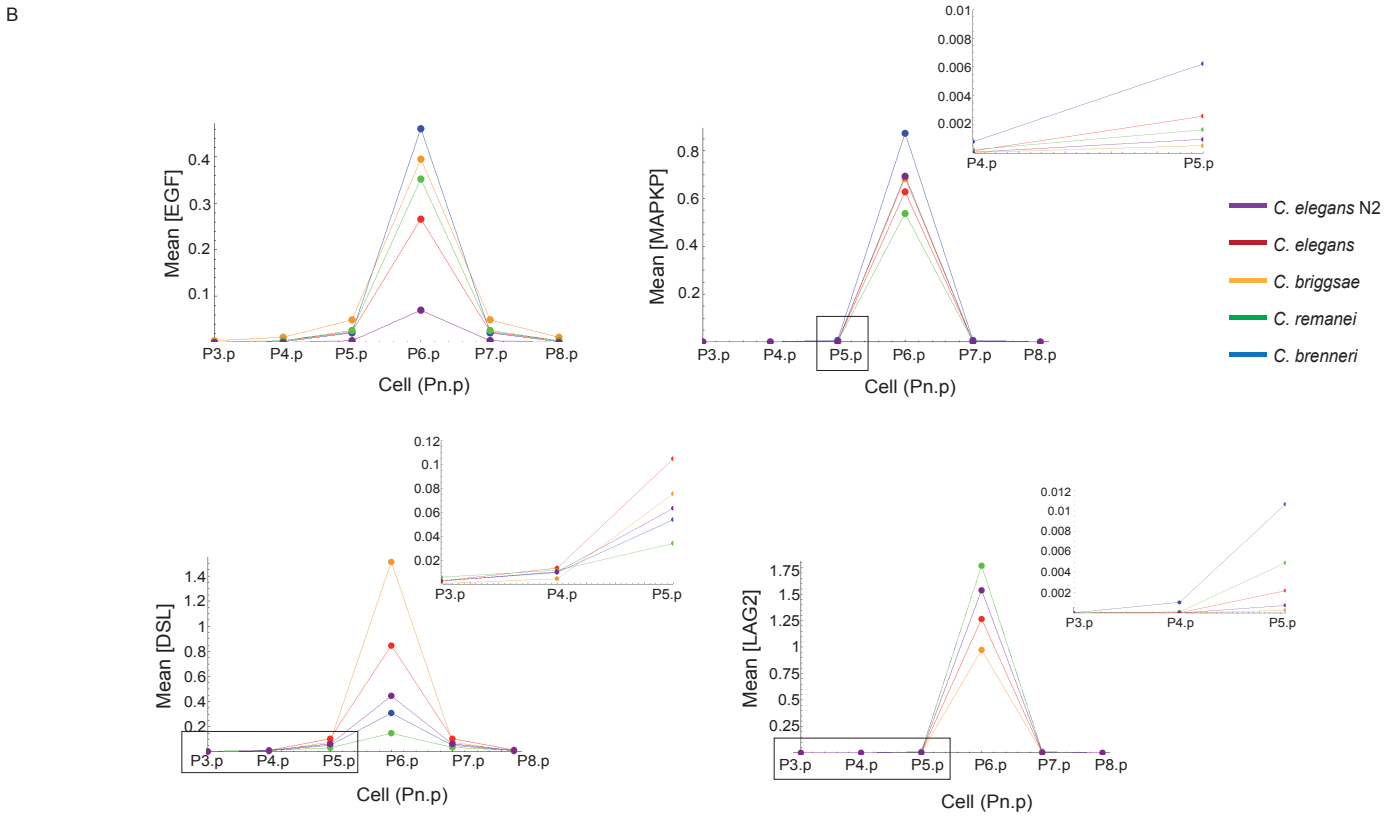

Protein	Mean expression ratio in P6.p/P5.p				
	C. elegans N2	*C. elegans*	*C. briggsae*	*C. remanei*	*C. brenneri*
EGF	63	45	29	35	53
MAPKP	$1.4x10^{6}$	158.166	$3x10^{6}$	112.185	25.670
LAG2	$6\ x10^{22}$	$5.6\ x10^{15}$	$1\ x10^{25}$	$1.4\ x10^{18}$	$9.6\ x10^{14}$
DSL	10	20	33	11	12

Figure S4

Figure S5

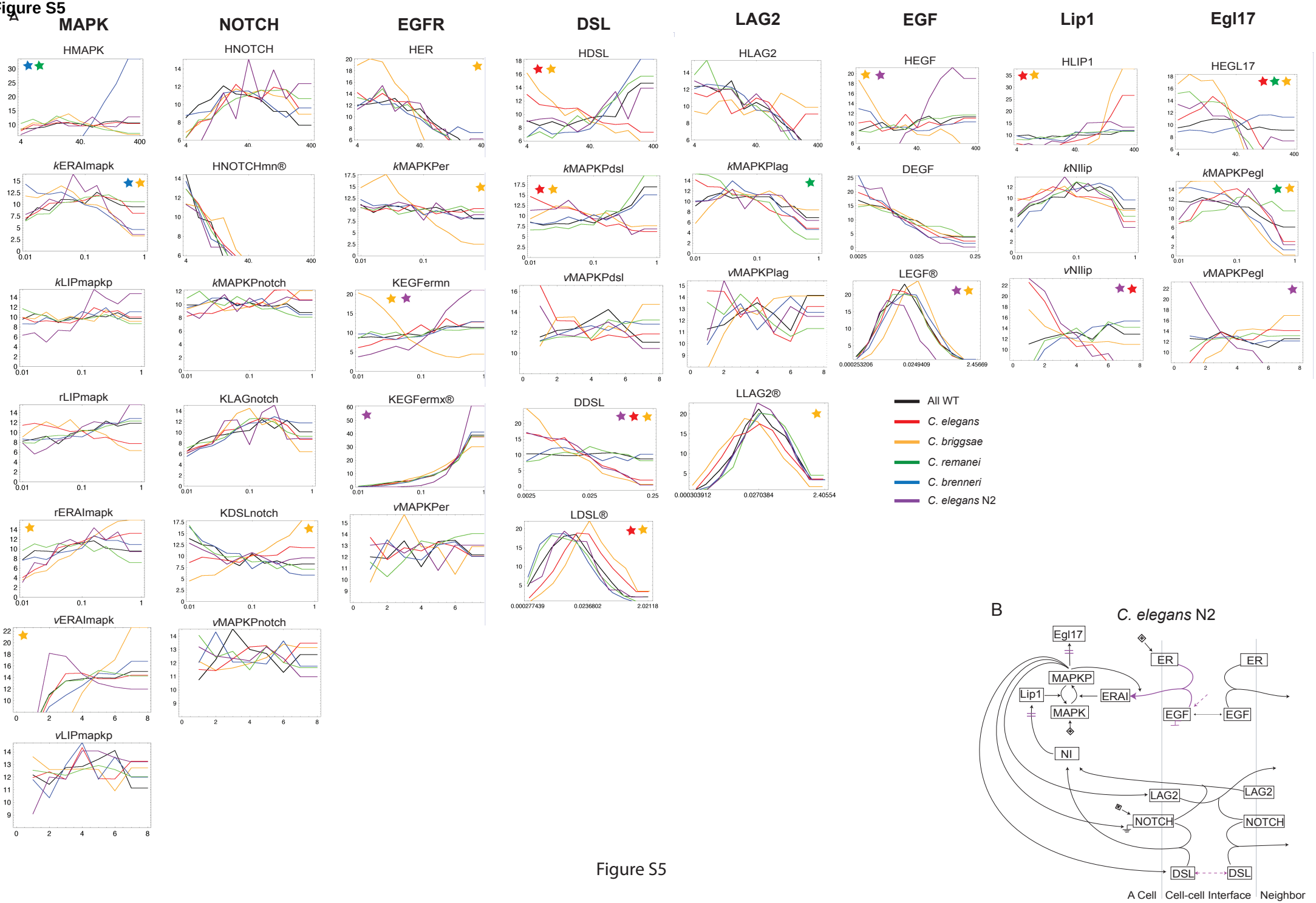

Figure S5

Figure S6

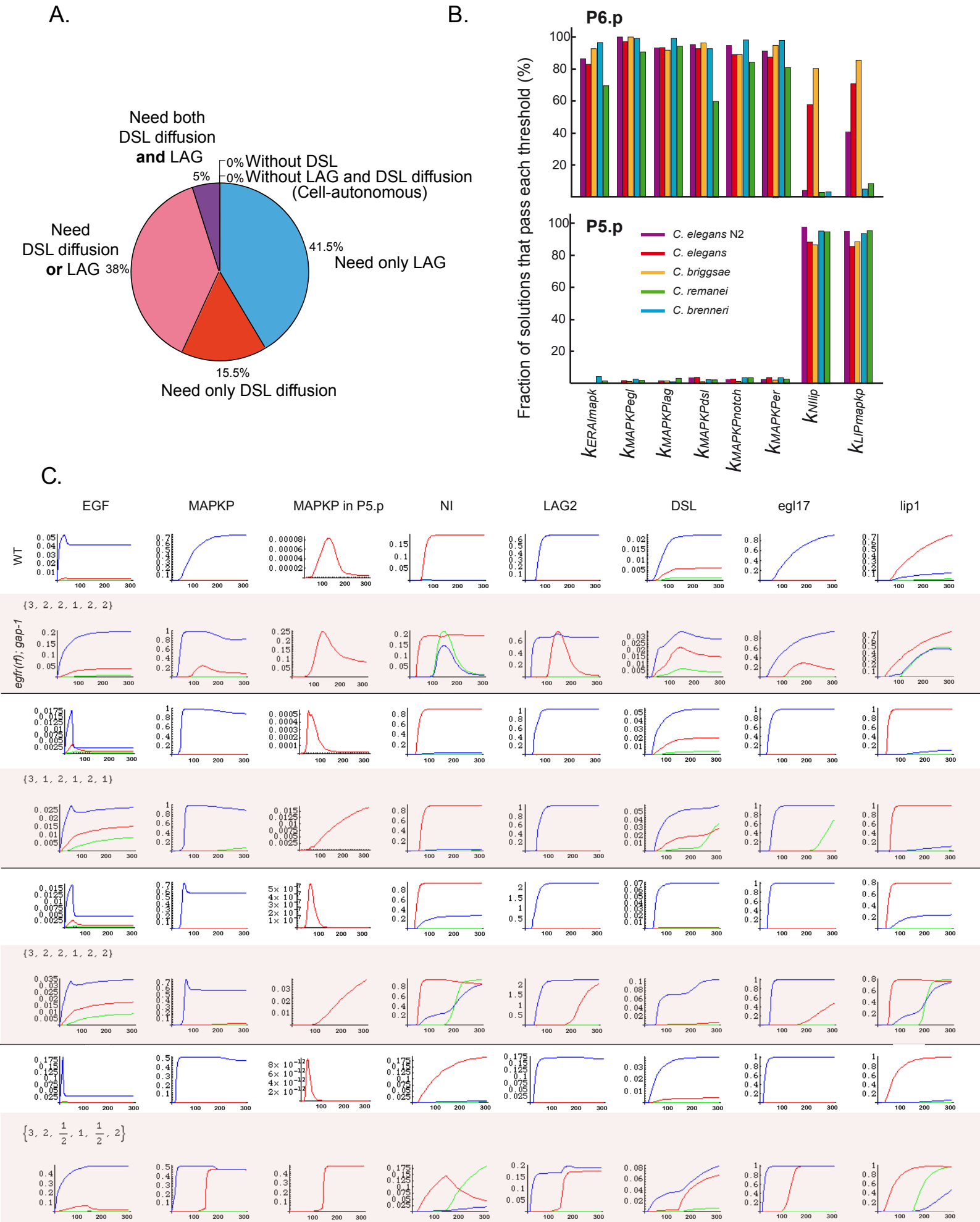

Figure S6

Supplementary Information

for:

Quantitative variation in autocrine signaling and pathway crosstalk within the *C. elegans* vulva specification network

Erika Hoyos*, Kerry Kim* Josselin Milloz, Michalis Barkoulas, Jean-Baptiste Pénigault, Edwin Munro, Marie-Anne Félix

*: These authors contributed equally

Supplemental Figures

Figure S1. Characteristics of wild-type solutions. ***Related to Figure 1.***
(A) Network diagram (left) indicating the strength of the interactions characteristic of parameter sets of wild-type solutions compared to random parameter sets. This network summarizes the Kolmogorov-Smirnov tests comparing parameter distributions of wild-type solutions against random solutions (Table S4). Thick solid lines in red indicate stronger interactions, and thin dotted lines weaker interactions. LAG2 synthesis rate (a) tended to be higher than random sets, whereas DSL and EGF synthesis and EGF diffusion rate (b-d) tended to be lower. We interpret these requirements by the fact that high rates of synthesis and diffusion of the diffusible ligands EGF and DSL may result in ectopic 1° or 2° fate adoption, while the membrane-bound LAG2 in one cell only activates Notch in adjacent cells. The histograms are in semi-logarithmic scale. Note that the parameters indicated by stars do not have a random (flat distribution) because their distribution is partially constrained by other free parameters (cf. Modeling Procedures). The significance of the parameter distributions obviously depends here on the explored range (cf. Modeling Procedures). However, the distributions of synthesis rates of the two Deltas (trans-membrane and diffusible) can be directly compared. Note that parameter distributions in other figures are compared to wild-type solutions as reference.
(B) Developmental time course for four model solutions. Concentration (y-axes) versus time (x-axes) for key nodes in the network in P6.p (blue), P5.p (red), and P4.p (green). One solution from each mode is displayed (the dynamics show variability among solutions and are not necessarily characteristic of the mode). Note the different scales for the y axes. Particularly variable features include: EGF distribution, presence of a transient increase in MAPKP/Egl17 in 2° cells, Notch/Lip1 activity in P6.p, respective concentrations of LAG2 and DSL, and DSL/Notch activity levels in 3° cells.

Figure S2. Switch behavior in the vulval induction network. *Related to Figure 2.*
(A) Experimental test of the effect on *osm-11* mutation on the fates of an isolated cell (P4.p, isolated by laser ablation). The wild-type and *dsl-1* data from Fig 2 are reproduced for reference. The proportion of the four fate classes differ between the wild type N2 and *osm-11* mutants (p= 0.004, χ^2 test). 1° and 2° fates appear reduced at the expense of 3° fates. We noted that *osm-11* mutant survival after laser cell ablation is low.
(B) Bifurcation diagram, signal response curve and fate planes for an isolated cell, corresponding to three different representative solutions that exhibit continuous behavior, a 2°-1° switch behavior or a 3°-2° and 2°-1° switch behavior (87, 8.4 and 2.3% of the solutions exhibiting the Isolated Cell behavior, respectively). Switch behavior is scored when changes in EGF produced little change in MAPKP level or cell fate marker expression until a threshold was reached, after which the cell abruptly changed to a different MAPKP level that was again stable over a wide range of EGF levels (see Supplemental Modeling Procedures). In the left panels, the bifurcation diagram shows the stability in the long-term concentrations of MAPKP, Lip1 and Egl17 as a function of EGF signal. Stable concentrations are represented by a solid line, and unstable by a dotted line. In the third case, a Hopf bifurcation occurs in the transition from the 3° to the 2° cell fate. In the right panels, the signal response graph shows the concentrations (at 300 min) of Lip1 (red) and MAPKP (blue) for increasing doses of EGF; the fate plane shows the cell 3°→2°→1° trajectory for increasing EGF (green curve).

Figure S3. Parameter distributions for different modes of vulval patterning and for solutions that stabilize a single cell in any of the three fates. *Related to Figure 3.*

(A) Each graph represents the distribution of values for a given parameter in the model: number of solutions (y-axes) vs. parameter value (x-axes) (n=1900 solutions of each category). The histograms are in semi-logarithmic scale, except for the cooperativities (*v* parameters) in linear scale. Each parameter value was sorted into one of ten (eight for cooperativities) evenly sized bins. Colored stars indicate the parameters with the largest significant differences between each mode and the pool of all wild-type solutions (98.1% of them belonging to the exclusively sequential mode), after a statistical comparison using the Kolmogorov-Smirnov test (see Table S4). ® indicates semi-free parameters with ranges limited by a previous free parameter (see Modeling Procedures).

(B) Patterning modes and isolated cell behavior. The "Isolated Cell" solutions were classified in the middle column among the four patterning modes of the first column. The percentage of solutions of each mode that reproduce the Isolated Cell behavior is indicated in the rightmost column. Note that in experiments with an isolated cell, this cell may adopt a variety of cell positions, much more so than P5.p / P7.p in intact worms. In our modeled isolated cell, it was thus appropriate not to enforce the EGF concentration that would be seen by P5.p and P7.p in the six-cell row in those solutions.

Figure S4. Spatial profile and amplification in the MAPK pathway. *Related to Figure 4.*

(A) Average concentration of EGF, MAPKP, LAG2 and DSL in each Pn.p cell, at the time when the concentration was maximum in P6.p. The table entries indicate the mean ratio between protein level in P6.p over P5.p (n=500 for each mode). The patterning modes differed significantly (repeated measures ANOVA, ratio of EGF levels in P6.p over P5.p X patterning mechanism interaction, $F_{3,\infty}$=19, p<<0.001; repeated measures ANOVA on Log-transformed data, ratio of MAPKP levels in P6.p over P5.p X patterning mechanism interaction, $F_{3,\infty}$=374, p<<0.001; repeated measures ANOVA on Log-transformed data, ratio of LAG2 levels in P6.p over P5.p X patterning mechanism interaction, $F_{3,\infty}$=237, p<<0.001; repeated measures ANOVA, ratio of DSL levels in P6.p over P5.p X patterning mechanism interaction, $F_{3,\infty}$=168, p<<0.001). The EGF level ratio is lowest in the *both required* mode (fast EGF diffusion), where 2° fate specification requires autocrine DSL signaling in P(5,7).p and lateral paracrine induction by P6.p (LAG2 and DSL). A low EGF level ratio in P6.p over P5.p may compromise P6.p capacity to laterally induce the 2° fate, which explains the need for some morphogen-based induction. DSL expression in these solutions is also much lower than in solutions that use the *exclusively morphogen* mode. Thus, both mechanisms of induction can cooperate to generate the wild-type pattern when MAPKP activity and Delta expression in P(5-7).p cells are each individually too weak.

(B) Same as in (A), but for the different *Caenorhabditis* species solutions (n=500 for each species). The species also differed in the ratio of expression (repeated measures ANOVA, ratio of EGF levels in P6.p over P5.p X *Caenorhabditis* species interaction, $F_{3,\infty}$=20.5, p<<0.001; repeated measures ANOVA on Log-transformed data, ratio of MAPKP levels in P6.p over P5.p X *Caenorhabditis* species interaction, $F_{3,\infty}$=41.1, p<<0.001; repeated measures ANOVA on Log-transformed data, ratio of LAG2 levels in P6.p over P5.p X *Caenorhabditis* species interaction, $F_{3,\infty}$=35, p<<0.001; repeated measures ANOVA, ratio of DSL levels in P6.p over P5.p X *Caenorhabditis* species interaction, $F_{3,\infty}$=84.4, p<<0.001; neither test included *C. elegans* N2).

Figure S5. Parameter distributions in the different *Caenorhabditis* species sets. *Related to Figure 5.*

(A) As in Fig S3, but the curves correspond to histograms of parameter distributions in solutions that correspond to the different *Caenorhabditis* species criteria (n=3600 solutions for each *Caenorhabditis* species and all wild-type solutions, n=583 for *C. elegans* N2). Colored stars indicate the parameters with the largest significant differences between a species set and all wild-type solutions using the Kolmogorov-Smirnov test (see Table S7A).

(B) Network diagram indicating the strength of interactions characteristic of *C. elegans* N2. Thick solid lines indicate stronger interactions, and thin dotted lines weaker interactions. The dotted arrow pointing to a node (e.g. EGF) means low synthesis. The = sign on an arrow indicates low cooperativity (or linearity) for that interaction.

Figure S6. Requirement for DSL and LAG2 in *C. briggsae* and titration effect by the EGFR in *C. elegans* N2 in the model. *Related to Figure 5.*

(A) Piechart showing the percentage of *C. briggsae* solutions that produce the 3°-3°-2°-2°-2°-3° pattern after AC ablation and the indicated DSL or LAG2 perturbation. n=200 *C. briggsae* solutions. Note that we did not find any *C. briggsae* solution that could use the *exclusively morphogen* mode (Figure 6A), which at first appears in contrast with the observation that these solutions, along with the *C. elegans* solutions, were the ones capable to stabilize an isolated 2° cell at intermediate EGF levels. The *C. briggsae* set was small (0.54% of solutions) and presented some extreme properties like strong activation and binding to Notch of DSL and a steep LAG2 concentration difference between P6.p and its neighbors.

(B) Percentage of solutions corresponding to each species set for which a given event occurs in P6.p (upper panel) or P5.p (lower panel), as in Figure 4B. n=500 solutions from each species.

(C) Timecourse of four solutions of the "*C. elegans* N2" set in the *egfr(rf); gap-1* double mutant. Concentration (y-axes) versus time (x-axes) for key nodes in the network in P6.p (blue), P5.p (red), and P4.p (green). For each parameter set, the time series are shown under wild-type conditions (WT, on white background) and under this perturbation (orange-shaded). The P(3-8).p fate pattern under the perturbation is indicated on the left between brackets. The EGF concentration is increased in distal cells, i.e. P5.p or even P4.p, and hyperinduction results from MAPK pathway activation in P5.p (sets #1, 2, 4) or P4.p (set #3).

Supplemental Tables

Table S1. Stable cell fate patterns produced by the model. *Related to Figure 1.*

Stable Cell Fate Pattern	% Occurrence
3° 3° 3° 3° 3° 3°	19%
2° 2° 2° 2° 2° 2°	11%
3° 3° 2° 1° 2° 3° (wild-type)	9%
1° 1° 1° 1° 1° 1°	6%
3° 3° 3° 1° 3° 3°	5%
3° 2° 2° 2° 2° 2°	4%
…	…
2° 1° 2° 1° 2° 1°	0.12%
All others	46%

In runs of the model with random parameters, 82% (n=20,000) sets produced cell fate patterns that were stable from 300 to 400 minutes of simulation. Listed are the most common patterns and their frequency of occurrence among these stable runs. The final hit rate for the stable wild-type pattern is 7.4% (82% x 9%).

Table S2. Role of *dsl-1* in 2° fate specification of an isolated cell. *Related to Figure 2*.

A. Laser ablation: Isolation of P4.p

Fate	Lineage	*dsl-1(+)*	*dsl-1(0)*
1°	TTTT	11	22
	TTTO	3	4
	TTOT		1
	TTOO	1	
	TTDD	1	
1°/3°	OT S	2	1
	sLTT	1	
1°/2°	TTTU	1	1
	TTUT	1	
	TTTL	2	7
	TODL		1
	OTTL		
	TTLL	6	3
	OTLL		1
	DDLL	1	
	TTLL	1	
	TTUL	1	1
	LTTT		3
	LLTO	1	
	TDLL	1	
2°	LLTU	6	1
	LTLU	1	
	LLTL	1	
	LTTU	1	
2°/3°	LT S		
3° or F	S S	5	4
	F		2
Total		48	52

B. "Genetic" ablation of Pn.p cells using *unc-84* mutant animals

Fate	Lineage	*dsl-1(+)*	*dsl-1(0)*
1°	TTTT	37	51
	TTTO		6
	OTTO		2
	TTOO	2	
	TOOO		1
	DTTD	1	
	TOOT	1	
	TTTV	2	5
	TTT?		1
	TTTs		1
1°/3°	TT S	1	1
	OO S		1
1°/2°	TTLL	8	2
	LTTU		1
	LTTU	1	
	TTTU		2
	TTUT	1	2
	TTUO		1
	TTTL		5
	TTTL	4	1
	TTTD		1
	LTTV		1
	OTDL		1

	LUDD		1
	TOUT	1	
	DDUO	1	
2°	LLTU	7	1
	LTTL	2	
	LTTL	2	
	LTTL		1
	LLLU	1	
	LTTU	1	
	LOTL	1	
	LTOL	1	
	LOTL	1	
	LULL	1	
	LTUL	1	
	LLTL	1	
	UTTU		2
	TUTU		1
2°/3°	LL S	1	
	LL S	2	
	UT S	1	
	LO S	1	
3°	S S	2	1
	S ss	1	
	ssss	1	1
?	?	3	1
	S DD	1	
Total		92	95

(A) Cell fate and lineage pattern of an isolated P4.p cell in *dsl-1(+)* vs. *dsl-1(ok180null)* worms. P3.p and P(5-8).p were ablated at the late L1 stage or early L2 stage. (B) Cell fate and lineage pattern of an isolated Pn.p cell in *dsl-1(+)* vs. *dsl-1(ok180null)* worms in a *unc-84(e1410)* background at 23°C (see Experimental Procedures). The orientation of P4.p granddaughter divisions is indicated. T: transverse (left-right); L: longitudinal (antero-posterior); O: oblique, D: divided. S (s):half (quarter) 3°. F: Pn.p fusion to hyp7 in the L2 stage without division (Eisenmann et al., 1998). The two Pn.p daughters can adopt different sub-fates, hence the 1°/2° and 2°/3° categories. We classified any vulval (non-3°) sublineage with an adhesion to the cuticule (underlined in A-B) as 2°. We also scored LT as half 2°. The number of animals with a given cell lineage is indicated in the corresponding genotype column.

Table S3. Cell fate patterns after elimination of one patterning mechanism. ***Related to Figure 3.***

Mode	Perturbation	Pattern	Stable	Frequency (%)
Exclusively Sequential	No Lag2, no DSL diffusion	**3°3°3°1°3°3°**	Yes	**74.0**
		3°3°1°1°1°3°	Yes	8.3
		3°3°3°1°3°3°	No	4.1
	No EGF diffusion	3°3°2°1°2°3°	No	0.6
		3°3°2°1/2°2°3°	Yes	0.2
	Mosaic for EGFR	3°3°2°1°2°3°	No	0.9
		3°1/3°2°1°2°1/3°	Yes	0.5
Both Required	No Lag2, no DSL diffusion	**3°3°3°1°3°3°**	Yes	**38.0**
		3°3°3°1°3°3°	No	9.8
		3°3°1°1°1°3°	Yes	8.6
	No EGF diffusion	**3°3°2/3°1°2/3°3°**	Yes	**18.4**
		3°3°2°1°2°3°	No	13.7
		3°3°3°1°3°3°	Yes	11.5
	Mosaic for EGFR	3°3°2°1°2°3°	**No**	**30.6**
		3°3°2/3°1°2/3°3°	Yes	14.8
		3°3°3°1°3°3°	Yes	8.0
Fully Redundant	No Lag2, no DSL diffusion	No Failure		
	No EGF diffusion	3°3°2/3°1°2/3°3°	Yes	0.2
		3°3°2°1°2°3°	No	0.1
	Mosaic for EGFR	3°3°2°1°2°3°	No	5.6
		3°2/3°2°1°2°2/3°	Yes	4.6
Exclusively Morphogen	No Lag2, no DSL diffusion	No Failure		
	No EGF diffusion	**3°3°3°1°3°3°**	Yes	**66.0**
		3°3°2/3°1°2/3°3°	Yes	27.2
		3°3°2/3°1°2/3°3°	No	3.7
	Mosaic for EGFR	**3°3°3°1°3°3°**	Yes	**44.7**
		3°3°2/3°1°2/3°3°	Yes	19.8
		3°3°3°1°3°3°	No	4.7

Frequent failure patterns found when using the perturbation in the second column, which removes either the sequential (No Lag2, no DSL diffusion) mechanism or the morphogen-based (No EGF diffusion and Mosaic for EGFR) mechanism. Bold indicates the most frequent failures (either fate pattern or stability). Without lateral induction, the most common pattern was 3°-3°-3°-1°-3°-3°, but loss of lateral inhibition also yielded defective patterns such as the underlined 3°-3°-1°-1°-1°-3°. Without morphogen induction, a common pattern was an unstable wild-type where the wild-type pattern was not stably maintained from 300 to 400 min, or a 3°-3°-2/3°-1°-2/3°-3° pattern (intermediate fates between 2° and 3° in P(5,7).p, Fig 1C). These results indicate that both induction mechanisms cooperate to induce the 3°-to-2°

transition in P5.p and P7.p: lateral induction from P6.p induces the 2° fate in its neighbors, and morphogen induction tends to stabilize it.

Table S4. Mean parameter values for the different patterning modes. *Related to Figure 3.*

Pathway	Node	Parameter	Exclusively Sequential	Exclusively Morphogen	Fully Redundant	Both Required	Single Cell 3 fates
MAPK	EGF	H_{EGF}	90	76	78	125 (↑)	91
		L_{EGF}	0.05	0.09	0.08	0.04	0.05
		D_{EGF}	0.03	0.04	0.04	0.07 (↑)	0.03
	ER	H_{ER}	55	57	51	60	58
		$\kappa_{MAPKPer}$	0.21	0.23	0.23	0.24	0.21
		$K_{EGFermn}$	0.24	0.25	0.23	0.22	0.24
		$K_{EGFermx}$	0.51	0.47	0.46	0.45	0.51
		$\nu_{MAPKPer}$	4.7	4.6	4.6	4.6	4.5
	MAPK	H_{MAPK}	93	86	100	94	98
		$\kappa_{ERAImapk}$	0.21	0.20	0.21	0.24	0.16
		$\kappa_{LIPmapkp}$	0.22	0.24	0.26	0.22	0.25
		$r_{LIPmapk}$	0.24	0.18	0.21	0.22	0.15 (↓)
		$r_{ERAImapk}$	0.21	0.26	0.28 (↑)	0.24	0.27
		$\nu_{ERAImapk}$	5	3.4 (↓)	3.6 (↓)	4.3	5.3
		$\nu_{LIPmapkp}$	4.5	4.4	4.4	4.5	4.4
	Egl17	H_{EGL}	81	72	66	79	61
		$\kappa_{MAPKPegl}$	0.16	0.22 (↑)	0.17	0.13	0.19 (↑)
		$\nu_{MAPKPegl}$	4.4	5	5	4.4	5.2 (↑)
Notch	DSL	H_{DSL}	107	40 (↓)	49 (↓)	76	60 (↓)
		$\kappa_{MAPKPdsl}$	0.30	0.03 (↓)	0.06 (↓)	0.22	0.05 (↓)
		L_{DSL}	0.06	0.2 (↑)	0.17 (↑)	0.12 (↑)	0.16 (↑)
		D_{DSL}	0.05	0.02 (↓)	0.02 (↓)	0.05	0.03 (↓)
		$\nu_{MAPKPdsl}$	4.5	4.2	3.6 (↓)	4.4	4.1
	LAG2	H_{LAG}	70.5	120 (↑)	78	86	80
		$\kappa_{MAPKPlag}$	0.19	0.32 (↑)	0.28 (↑)	0.20	0.22
		L_{LAG}	0.16	0.04 (↓)	0.12	0.12 (↓)	0.13
		$\nu_{MAPKPlag}$	4.6	4.6	4.9	4.5	4.6
	Notch	H_{NOTCH}	78	41 (↓)	99	93	86
		$H_{NOTCHmn}$	14	9	12	18	13
		$\kappa_{MAPKPnotch}$	0.20	0.27 (↑)	0.24 (↑)	0.23	0.26 (↑)
		$K_{LAGnotch}$	0.24	0.21	0.23	0.22	0.21
		$K_{DSLnotch}$	0.19	0.25	0.21	0.22	0.20
		$\nu_{MAPKPnotch}$	4.5	4.7	4.8	4.6	4.8
	Lip1	H_{LIP}	94	94	126 (↑)	80	111
		κ_{Nllip}	0.22	0.35 (↑)	0.21	0.18	0.23
		ν_{Nllip}	4.6	4.7	4.7	4.8	4.5

Mean values of all model parameters for the different patterning modes. We tested each parameter distribution in each mode for significant departures from the overall distribution (Fig S3) using the Kolmogorov-Smirnov test. Very significant departures ($<10^{-15}$) are indicated with ↑ indicating a tendency for high values while ↓ indicates low values.

Table S5. Cell fate patterns produced after elimination of the *N* —| *M* crosstalk (Lip1-mediated MAPK dephosphorylation). *Related to Figure 4.*

Pattern	All Wild-type (%)	Exclusively Sequential (%)	Exclusively Morphogen (%)	Fully Redundant (%)	Both Required (%)
Wild-type	77.2	84.0	52.0	37.6	56.0
3° 2° 2° 1° 2° 2°	2.5	2.2	0.8	**14.2**	2.5
3° 2/3° 2° 1° 2° 2/3°	2.3	1.6	3.0	**9.0**	4.6
3° 3° 2° 1/2° 2° 3°	1.7	1.6	0.6	0.0	**7.2**
3° 2/3° 1° 1° 1° 2/3°	0.5	0.4	**6.2**	2.8	3.2
3° 2° 1° 1° 1° 2°	1.6	0.8	4.0	**9.8**	3.0
3° 3° 1/2° 1° 1/2° 3°	1.3	1.2	**8.0**	**7.6**	1.6
3° 3° 1° 1° 1° 3°	0.5	0.2	**16.0**	2.4	4.0

Percentage of occurrence of different patterns produced when MAPKP dephosphorylation by Lip1 is blocked, for each patterning mode. In bold are highlighted the most frequent failure patterns (> 5%). Additional unstable patterns were found, so percentages do not sum to 100. n=500 solutions for each mode and n=3000 for the wild-type set. The resulting pattern greatly depended on the patterning mode. Under the *exclusively morphogen* mode, most non-wild type patterns consisted of adjacent 1° fates in P(5,7).p (3°-3°-1°-1°-1°-3°), consistent with a block in classical lateral inhibition (Greenwald et al., 1983). However, in the other modes, this perturbation more often produced an abnormal 2° fate in either P6.p or P(4,8).p. In the *fully redundant* mode, we most often saw ectopic 2° fate induction in P(4,8).p, with a normal fate pattern for P(5-7).p (3°-2°-2°-1°-2°-2°). Failure rates were overall much lower in the *exclusively sequential* mode, yet most of them also concerned this 3° to 2° fate transformation of P(4,8).p. Thus, for solutions where lateral induction is sufficient, Lip1 normally acts in preventing 2° fate induction in distal cells through reduction in Delta production downstream of MAPKP. Finally, in the *both required* mode, removal of the *N* —| *M* crosstalk produced a 3°-3°-2°-1/2°-2°-3° fate pattern, affecting P6.p. In this case, P6.p required the inhibition of MAPK by Notch to produce a 1° fate. This unintuitive result is explained by the activation of the DSL loop after MAPK activation, which competes with 1° fate specification.

Table S6. Lineages in response to experimental *egf* overexpression in *C. elegans*. *Related to Figure 5A*.

A. JU1023. Vulval induction index = 3.008 (n=125).

P3.p	P4.p	P5.p	P6.p	P7.p	P8.p	n
S S or F	S S	LLTU	TTTT	UTLL	S S	124
F	+ TU	LLTU	TTUT	LL +	S S	1

B. JU1024. Vulval induction index = 3.01 (n=50).

P3.p	P4.p	P5.p	P6.p	P7.p	P8.p	n
S S or F	S S	LLTU	TTTT	UTLL	S S	49
F	S S	LLTU	TTTT	UTUT	LL S	1

C. JU1105. Vulval induction index = 3.06 (n=71).

P3.p	P4.p	P5.p	P6.p	P7.p	P8.p	n
S S or F	S S	LLTU	TTTT	UTLL	S S	26
F	S S	LLTU	TTTT	TTLL	S S	1
F	S +	LLTU	TTTT	UTLL	S S	1
F	LLTU	TTTT	TTTT	TTLL	S S	1
F	S S	LLTU	TTTT	LLLT	TTLL	1

D. JU957. Vulval induction index = 3.42 (n=72).

P3.p	P4.p	P5.p	P6.p	P7.p	P8.p	n
S S or F	S S	LLTU	TTTT	UTLL	S S	24
S UL	S S	LLTU	TTTT	UTLL	S S	1
S UL	S S	LLTU	TTTT	UTLL	S S	1
S TT	S S	LLTU	TTTT	UTLL	S S	1
ssTT	S S	LLTU	TTTT	UTLL	S S	1
4 cells	S S	LLTU	TTTT	UTLL	S S	1
LLLL	S S	LLTU	TTTT	UTLL	S S	1
LT S	S S	LLTU	TTTT	UTLL	S S	1
S S	TT S	LLTU	TTTT	UTLL	S S	1
S S	S LL?	LLTU	TTTT	UTLL	S S	1
S S	S OT	LLTT	TTTT	TTLL	S S	1
F	S TT	LLTU	TTTT	UTLL	S S	1
S S	S LT	LLTU	TTTT	UTLL	S S	1
S S	UT ?	LLTU	TTTT	UTLL	S S	1
S S	DS?	LLTU	TTTT	UTLL	S S	1
S S	S DD	DLTT	TTTT	UTLL	S S	1
S S	S TU	LLTT	TTTT	UTLL	S S	1
S S	S DU	LLTU	TTTT	UTLL	S S	1
ssTT	S S	LLTU	TTTT	UTLL	LL S	1
STO	S S	LLTO	TTTL	LLLL	S TT	1
S ss	S TT	LLTU	TTTT	UTLL	S S	1
STU	ssTT	LLTU	TTTT	UTLL	S S	1
LLUT	TTUT	LLTU	TTTT	UTLL	S S	1
S TU	UTTU	LLUU	TTTT	UTLL	S S	1

LUL?	S TT	LLTU	TTTT	UTLL	S S	1
S LT	UL S	8 nuclei	(TTTT)	(UTLL)	S S	1
S S	S TT	LLTD	TTTT	DTLL	S DD	1
S UT	S TT	ULUT	TTTT	ULLU	TT S	1

E. JU1100. Vulval induction index = 4.22 (n=30).

P3.p	P4.p	P5.p	P6.p	P7.p	P8.p	n
F or S S	S S	LLTU	TTTT	UTLL	SS	5
F	S S	LLTU	TTTT	TTDL	SS	1
F	S LL	TUTT	TTTT	UTLL	SS	1
S S	S S	LLTT	TTTT	TTUL	LL S	1
F	LTTT	TTTT	TTTT	UTLL	SS	1
F	LLTU	TTTT	TTTT	UTLL	SS	1
S S	"+"	"+"	"+"	"+"	SS	1
S S	"+"	"+"	"+"	"+"	SS	1
F	LTUT	TTDD	DDTT	UTLL	TU S	1
S S	LLTT	TTDD	DDDU	TTTU	TLss	1
S S	LLTT	TTTT	TTTL	LLLL	TU S	1
S UL	LTTU	TLLT	TTTT	TTLL	S S	1
S LL	TUTT	TUTT	TTTT	TTLL	S S	1
F	LOUL	DDTT	TTTT	TTDD	OTLL	1
S S	LLTU	TTTT	TTTT	TTDL	OTLL	1
S S	LLTU	TTTT	TTTT	TLTT	LLLL	1
F	LLTT	"+"	"+"	DDDL	UTLL	1
F	LLTT	"+"	"+"	"+"	TTLL	1
"+"	"+"	"+"	TOTT	UTLL	S S	1
S S	"+"	"+"	"+"	"+"	"+"	1
S sL	TLLL	UTTT	TTTT	TTTT	TLLL	1
S LL	TTLL	LTTT	TTTT	TTUT	TLLs	1
S sL	TTTL	LLTU	TTTT	TTTT	TTLL	1
LLOU	LLTT	TTTT	TTTT	DDDL	UL S	1
"+"	"+"	DDDD	TTTT	TTDD	DD S	1
S +	"+"	"+"	"+"	"+"	"+"	1
S +	"+"	"+"	"+"	"+"	"+"	1
LLUU	OTTU	UTTT	TTTT	UTLL	TTLL	1
LLUT	LLTT	"+"	"+"	"+"	"+"	1
LLTT	LUTT	TLTT	TTTT	TTTT	TULL	1
"+"	"+"	"+"	"+"	"+"	"+"	1

Vulval precursor cell fate lineages were scored as in Table S2 in five *C. elegans* transgenic lines expressing different *lin-3* levels in the anchor cell (see Supplemental Experimental Procedures). The number of corresponding animals is indicated on the right. “?” stands for not determined and “+” for induced. Vulval lineages of a line expressing still higher *lin-3* levels in the anchor cell is reported in Table 3 in Katz et al. (1995). See also Félix (2007) for vulva lineages of animals with *mfIs10[Cbr-lin-3]* in *C. elegans* N2 background (induction index in the 5.5-6.0 range). In *C. briggsae*, the first abnormal pattern upon mild *egf* overexpression is the adoption of 1° fates by P(5,7).p and of 2° fates by P(5,8).p, yielding a 3°-2°-1°-1°-1°-2° pattern (Félix, 2007) (this pattern was more frequent on the anterior side; note that we did not distinguish in the model the relative competence of anterior versus posterior Pn.p cells;

Clandinin et al., 1997). In contrast, in *C. elegans*, P(5,7).p retained their 2° fate while P(3,4,8).p adopted various induced fates (2° or 1°, or hybrid fates where the two daughters adopted different fates), without necessary alternation between 2° and 1° Pn.p fates. Thus, the *egf* overexpression pattern clearly distinguished experimentally the two species.

Table S7. Parameter values in the *Caenorhabditis* species sets and the search for N2. *Related to Figure 5B.*

A. Mean parameter values in the *Caenorhabditis* species sets.

Pathway	Node	Parameter	Wild-type	*C. elegans* N2	*C. elegans*	*C. briggsae*	*C. remanei*	*C. brenneri*
MAPK	EGF	H_{EGF}	87	150(↑)	90	61 (↓)	98	84
		L_{EGF}	0.06	0.01(↓)	0.05	0.08 (↑)	0.05	0.07
		D_{EGF}	0.031	0.014	0.025	0.032	0.033	0.019(↓)
	ER	H_{ER}	60	57	55	21 (↓)	54	68
		$\kappa_{MAPKPer}$	0.20	0.19	0.20	0.10 (↓)	0.20	0.20
		$K_{EGFermn}$	0.25	0.36(↑)	0.26	0.11 (↓)	0.24	0.24
		$K_{EGFermx}$	0.50	0.68(↑)	0.51	0.46	0.49	0.53
	MAPK	H_{MAPK}	94	97	90	72	70 (↓)	192 (↑)
		$r_{ERAImapk}$	0.21	0.24	0.26	0.32 (↑)	0.20	0.24
		$r_{LIPmapk}$	0.24	0.28	0.18	0.18	0.24	0.25
		$v_{ERAImapk}$	5.0	4.4	5.0	6.1 (↑)	4.8	5.2
		$\kappa_{ERAImapk}$	0.22	0.16	0.21	0.14 (↓)	0.23	0.15 (↓)
	Egl17	H_{EGL}	81	67	51 (↓)	24 (↓)	44 (↓)	97
		$\kappa_{MAPKPegl}$	0.15	0.16	0.16	0.08 (↓)	0.20 (↑)	0.10
		$v_{MAPKPegl}$	4.4	3.6(↓)	4.8	5.2 (↑)	4.7	4.4
Notch	DSL	H_{DSL}	110	100	73 (↓)	63 (↓)	114	121
		$\kappa_{MAPKPdsl}$	0.28	0.17	0.16 (↓)	0.18 (↓)	0.32	0.26
		L_{DSL}	0.06	0.06	0.13 (↑)	0.18 (↑)	0.05	0.03
		D_{DSL}	0.05	0.02(↓)	0.02 (↓)	0.02 (↓)	0.05	0.05
	LAG2	$\kappa_{MAPKPlag}$	0.19	0.18	0.16	0.21	0.12 (↓)	0.16
		L_{LAG}	0.17	0.16	0.15	0.10 (↓)	0.20	0.18
	Notch	$K_{DSLnotch}$	0.18	0.20	0.24	0.3 (↑)	0.17	0.15
		$H_{NOTCHmn}$	14.4	15	19.5	23.5(↑)	16.0	13.1
	Lip1	H_{LIP}	95	115	151 (↑)	198 (↑)	98	97
		v_{NIlip}	4.6	3.4 (↓)	3.6 (↓)	4.1	4.8	5.1

Mean values of parameters for each species set. ↑ indicates a tendency for high values, while ↓ indicates low values, for parameters with distributions that were significantly different between at least one *Caenorhabditis* species and all wild-type solutions (shown in colors in Fig 5B), with Bonferroni corrected $P < 10^{-15}$. *C. elegans* and *C. briggsae* solutions reproduced both EGF overexpression and AC ablation experiments (Fig 5A). N=3000 solutions for each group, except N=583 solutions for comparisons with *C. elegans* N2.

B. Further tests, including those used to define the *"C. elegans* N2" solutions.

Perturbation	**Expected result** **(Reference)**	**All wild-type** N=667000	***C. briggsae*** N=3620	***C. elegans*** N=43530	***C. elegans* N2** N=583	***C. brenneri*** N=57638	***C. remanei*** N=193302
Qualitative reporter data	$[Lip1]_{P6.p}<0.5[Lip1]_{P(5,7).p}$ $[Egl17]_{P6.p}>0.5[Egl17]_{P(5,7).p}$ (1)	79	7	31	100*	90	96
Halve *egf* dose	Wild-type(2)	70	76	69	100*	96	66
lin-15 mutant	P(5-7).p: 2° 1° 2° & at least half 1° in P3.p or P4.p or P8.p(3)	18	9	11	100*	25	16
dsl mutant	Wild-type(4)	89	79	86	100*	95	97
EGFR mosaic	Wild-type(5)	95	99	96	100*	93	96
egfr(rf)/gap-1(0)	P6.p: 1° & P4.p or P8.p induced: 1°, 2°, 1/2°, 1/3°(6)	32	27	35	100*	27	28
Notch knockout	3° 3° 1° 1° 1° 3° with 1- 3 ACs (7)	58	53	55	36	79	48
No EGF diffusion	Wild-type	97	99	98	100	99.8	97
No Lag-2	Wild-type	13	54	44	26	9	6
No DSL diffusion	Wild-type	80	75	73	91	89	88

* We required a parameter set to satisfy this requirement to be classified as *C. elegans N2* (final set of N=583).

Percentage of solutions of each column passing a given test. The "*C. elegans* N2" set was defined by parameter sets satisfying all behaviors marked with *. A "C. elegans N2 preliminary" set was defined as passing the five first tests (see Modeling Procedures). Note that we enforced a fully wild-type pattern in the EGFR mosaic experiments for *C. elegans* N2. References: (1) (Milloz et al., 2008); (2) (Ferguson and Horvitz, 1985); (3) (Sternberg, 1988; Sternberg and Horvitz, 1989); (4) (Chen and Greenwald, 2004); (5) (Koga and Ohshima, 1995; Simske and Kim, 1995); (6) (Hajnal et al., 1997); (7) (Greenwald et al., 1983; Sternberg and Horvitz, 1989).

Table S8. Evolution of 2° fate specification of an isolated cell. *Related to Figure 6.*

Fate	Lineage	*C. elegans* N2	*C. briggsae* AF16	*C. remanei* JU825	*C. remanei* JU724	*C. brenneri* CB5161
1°	TTTT	7	14	9	13	17
	LTTT	2		1		1
	TTTL	2	2	1		
	OOOO	1	1			
	LTTL			1		
1°/3°	TTTS					1
	S TT					1
	TT S	1			1	2
1°/2°	TTTL	1	1	1		
	LTTT	1			4	
	LLTT	5				
	LTTL				1	
	LLTT		2			
	TTLL		1			
	LLTL		1			
	TTLL		2		2	1
	LTTL	1				
	OTTT	1				
	DDUD					
	TTUL		1			
	TTLU	1				
	UTTU		1			
	LOTT	1				
2°	UTLL	6	3			
	UTLL		1			
	UDTL		1			
	LTUL		1			
	LULU			1		
	LLTL					1
	LOOU	1				
	LTOU	1				
	LTUT	1				
	LLUU	1				
	ULTT	1				
1°/2°/3°	sTTL			1		
2°/3°	LL S		1			
3°	S S	2	3	12	17	9
Total		37	36	27	38	33

Cell fate and lineage pattern of an isolated P8.p cell in different *Caenorhabditis* species. The orientation of P8.p granddaughter divisions is scored as in Table S2.

Supplemental Experimental Procedures

Modeling Procedures

Abbreviations

ER: EGFR
ERAI: Internalized active EGF receptor (or Ras pathway component)
MAPK: MAP kinase
MAPKP: phosphorylated MAP Kinase
Egl17: 1° cell fate effector
DSL: diffusible Delta
LAG2: membrane-bound Delta
NOTCH: Notch receptor (LIN-12)
NI: Notch intracellular domain
Lip1: 2° cell fate effector and MAP kinase phosphatase
VPC: Vulva Precursor Cell
AC: Anchor Cell
$M \circlearrowleft$: positive intracellular feedback loop in MAPK pathway
$M \rightarrow N$: positive cell-autonomous crosstalk of MAP kinase pathway activating Notch pathway through DSL secretion
$M \dashv N$: negative intracellular crosstalk of MAP Kinase pathway inhibiting Notch pathway
$N \dashv M$: negative intracellular crosstalk of Notch pathway inhibiting MAP Kinase pathway.

Molecular interactions in the vulval induction network

In this section, we summarize the current biological understanding of vulval patterning, and justify the connections shown in Fig 1B as reasonable approximations of the real biological system. We designate the actual *C. elegans* proteins by their conventional gene names with a hyphen (e.g. LIN-3, LAG-2), whereas the model names (which often represent several molecular species) use a generic name for the molecule (e.g. EGF) or are distinguished by the absence of a hyphen (e.g. LAG2).

Our model attempts to include all known interactions, crosstalk and feedback determined by experiments (Sternberg, 2005). Briefly, the anchor cell (AC) releases the LIN-3/EGF ligand, a presumptive morphogen (Yoo et al., 2004) onto the row of vulval precursor cells (VPCs). This results in increased MAP kinase activity in cells where EGF binds to the EGF receptor, which ultimately activates MAPK. This, in turn, induces a 1° fate when the EGF signal is sufficiently high and triggers lateral signaling (trans-membrane and diffusible Deltas). These ligands bind to LIN-12/Notch receptors on neighboring cells and cause them to assume a 2° fate. We will review each step in more detail.

In the model, EGF is synthesized on P6.p and we allow EGF to diffuse to neighboring cells. All VPCs express the EGF receptor LET-23 (abbreviated ER in the model) that, upon binding of EGF is internalized and activates the Ras cascade (SEM-5, LET-60, LIN-45, etc.), ultimately activating MAP kinase (MAPK) by phosphorylation. Our model does not represent intermediates in this cascade: ER activation by EGF produces internalized ER (ERAI), which directly activates MAPK phosphorylation in the model. EGF is consumed when activating ER in the model.

High levels of phosphorylated MAPK (MAPKP) activate several genes involved in cell fate specification. MAPKP activates transcription of Egl17, a 1° cell fate effector in our model. Egl17 is named after *egl-17*, whose regulatory regions are commonly used as a 1° cell fate reporter (Burdine et al., 1997; Inoue et al., 2002; Yoo et al., 2004); yet note that EGL-17 itself (a FGF molecule) has no bearing on vulval epidermal fates. MAPKP activity is known to increase sensitivity to EGF through DEP-1 and EPS-8. EPS-8 production is activated by MAPKP and stabilizes the EGF receptor (Stetak et al., 2006). MAPKP activity blocks production of the EGFR phosphatase DEP-1 (Berset et al., 2005). Both DEP-1 and EPS-8 result in positive feedback loops whereby MAPKP activity results in increased sensitivity to EGF. We approximate these activities in the model with a single positive feedback where MAPKP directly increases the affinity of the EGF receptors for EGF. We explored models with two positive feedback loops (to separately simulate DEP-1 and EPS-8) and found no alteration in its ability to reproduce lifelike behavior.

Phosphorylated MAPK causes production of LIN-12/Notch ligands and degradation of Notch receptors. At least three functionally redundant Notch ligands (collectively called Deltas) have been identified: APX-1, DSL-1 and LAG-2 (Chen and Greenwald, 2004) (see also Komatsu et al., 2008). LAG-2 and APX-1 are membrane-bound and likely activate Notch receptors only on adjacent cells. DSL-1 (and possibly other DSLs) is secreted and thus should be able to bind to Notch receptors in distant cells as well as on the cell that produced it (autocrine signaling). In our model, MAPKP activity triggers the production of two Delta forms: one is diffusible (DSL, representing DSL-1 and any other diffusible Notch ligands) and can activate Notch on the cell that produced it or diffuse to neighboring or distant cells to activate Notch; the other is membrane-bound (LAG2, representing LAG-2 and APX-1), does not diffuse and activates Notch only on adjacent cells. In addition, MAPKP activity leads to post-translational degradation of Notch molecules in the cell (Shaye and Greenwald, 2002). In the model, Notch degradation is increased in response to high MAPKP.

Lateral signaling through Notch receptor activation induces a 2° fate. Upon ligand binding (DSL or LAG2 in the model), the Notch receptor is cleaved, producing an active intracellular fragment (NI) that activates Lip1 production. Lip1 causes dephosphorylation of MAPKP, antagonizing the EGF signal (Berset et al., 2001) and Lip1 is also a 2° fate effector. It is speculated that Notch down-regulation in P6.p may be necessary for the expression or activity of LAG-2 (Sundaram, 2005). We constructed models incorporating such behavior (as in equation (13)), and found that it decreased the frequency of finding wild-type solutions in a random search. Because this interaction is not proven, we focused our analysis on the network that did not include this interaction. Moreover, we could reconstitute the phenotype upon the Notch degradation block with the present network, so the ability to reproduce the experiment does not hinge upon this activity.

Linear cascades (such as SEM-5→LET-60→ …→MAPKP, MAPKP -| DEP -| ER, and MAPKP→Egl-17) are truncated in the model: the first element in the cascade directly activates the last. We offer three justifications for this truncation being reasonable: (1) We explored models that incorporated some of the intermediates and found no alteration in the model's ability to reproduce lifelike behavior. (2) Long cascades may have strong non-linearities and temporal delays between upstream activation and downstream response. We allow steep non-linearities in our model, and brief temporal delays are present as regulators must accumulate before reaching a threshold for maximal effect. Thus, our model can

approximate the behavior of these cascades. (3) The quantitative kinetics of these pathways have not been measured (and some pathways, such as the intermediates between MAPKP and *egl-17* are undetermined), so we do not think this additional complexity is useful to simulate. Though the linear cascades are truncated, the known feedback loops and crosstalks (both positive and negative) are present in the model.

Mathematical formulation of the model

The model is a system of differential equations that describes how the concentrations of protein in each cell or cellular compartment change with time. We simulate a row of six cells, all with identical networks, but differing in the EGF dose that they receive from the simulated AC. In each cell, the concentrations of proteins can vary independently. We assume that the concentration of a protein determines its activity (rather than some other metric, such as the absolute number of molecules) and that cells (or cellular compartments) are well-stirred reaction environments.

Each equation in the model describes the rate of change for a molecular concentration in a cell or cellular compartment. The rate of change is the sum of synthesis, decay, and conversion/transport processes (Kim, 2009; Meir et al., 2002b; von Dassow et al., 2000). Degradation, exo/endocytosis, binding, and unbinding follow 1st or 2nd order mass-action kinetics. Diffusible molecules (EGF, DSL) can move to neighboring compartments. We assume that the diffusion rate is the same regardless of position (i.e. the VPCs are regularly spaced, with no kinks or barriers to EGF diffusion along the VPC axis). While this is a coarse approximation of diffusion (one compartment per cell), this is a reasonable simplification because the details of diffusion rates and the diffusional boundaries are unknown. The kinetics of processes, whether transcriptional or post-transcriptional, such as enzyme activity and transcriptional activation, are constructed from Hill functions:

$$\frac{dX_i}{dt} \propto \Phi(A_i, \kappa_{Ax}, \nu_{Ax}) = \frac{A_i^{\nu_{Ax}}}{A_i^{\nu_{Ax}} + \kappa_{Ax}^{\nu_{Ax}}} \qquad \text{(S1)}$$

where A_i is the concentration of the activator in cell *i*, X_i is the molecule produced by *A*, Φ is the Hill function, ν_{Ax} is the apparent cooperativity for the process, and κ_{Ax} is the concentration of *A* where synthesis is half-maximal. We use Hill functions because they can be tuned to capture a wide range of activation curves and saturate at high levels. As an optimization to increase the speed of numerical integration, we restricted cooperativities (ν parameters) to integer values. We did not notice any difference in model behavior when this constraint was relaxed.

At the start of the simulation (time 0), all concentrations were 0, except for EGF receptor, Notch, and MAPK (unphosphorylated), which were maximal (value = 1). To simulate the anchor cell, *egf* message was placed only in the cell corresponding to P6.p; this resulted in exclusive production of EGF in this cellular compartment. At time 0, EGF began to be synthesized in P6.p, its concentration slowly rising over time until synthesis balanced degradation/transport. Diffusible proteins (EGF, DSL) could diffuse between adjacent cells.

Fate plane

Each cell fate was assigned according to Fig 1C. This fate plane determines cell fate as a function of the concentration of the fate effectors (named Egl17 and Lip1 after the pathway transcriptional reporters *egl-17* and *lip-1*). Although these thresholds are arbitrary, they still allow a great deal of flexibility in the MAPK and Notch activities, as the activation kinetics and thresholds of Egl17 and Lip1 are free parameters

(downstream of Mapk and Notch activation), and can vary between species. We did not parametrize the fate plane itself, because these additional parameters would have been redundant with those concerning Egl17 and Lip1 activation and degradation. For example, parametrization of the minimum fate effector concentration for the 2° and 1° fate (here fixed at 0.2) would not have been different from changing the fate effector half-life or ease of activation. We explicitly allowed intermediate cell fates, such as 1/2°, as observed experimentally (Tables S2, S6, S8) (Katz et al. 1995; Félix, 2007), especially because they were required to describe the anchor cell ablation in *C. elegans*.

List of model equations

In the equations below, all molecular concentrations are given by the molecule name in capital letters, followed by a subscript *i* indicating the cell or cellular compartment. In the 6-VPC model, P3.p through P8.p correspond to i=1 through 6, respectively. To avoid edge effects, we simulate 6 additional compartments (3 on each side) as empty cells that lack all synthesis and inductive/lateral signaling molecules, except for allowing EGF and DSL to diffuse through these compartments. We found six such compartments sufficient for our simulations, as incorporation of additional empty compartments did not alter our results.

Notation:

i = Cell or cellular compartment. In the 6-cell model, *i* = -2 to 9, with VPCs corresponding to *i* = 1 to 6 and the remaining values representing empty diffusional compartments. In the 1-cell model, *i* = -2 to 4, with the isolated VPC corresponding to *i* =1 and the remaining values representing empty diffusional compartments.

X_i =Concentration of molecule *X* in cell *i*. In the 6-cell model, concentrations of non-diffusible entities are always 0 when *i* < 1 or *i* > 6, because only 6 VPCs are present. In the 1-cell model, concentrations of non-diffusible entities are always 0 unless *i* = 1.

$$X_{adj(i)} = \text{Average concentration of} X \text{ on cells adjacent to cell} i = \frac{X_{i-1} + X_{i+1}}{2}$$

$$\Psi = 1 - \Phi$$

$$\frac{dER_i}{dt} = L_{ER} - ER_i EGF_i\left(\left(K_{EGFermx} - K_{EGFermn}\right)\Phi\left(MAPKP_i, \kappa_{MAPKPer}, \nu_{MAPKPer}\right) + K_{EGFermn}\right) - \frac{ER_i}{H_{ER}} \quad (1)$$

$$\frac{dERAI_i}{dt} = ER_i EGF_i\left(\left(K_{EGFermx} - K_{EGFermn}\right)\Phi\left(MAPKP_i, \kappa_{MAPKPer}, \nu_{MAPKPer}\right) + K_{EGFermn}\right) - \frac{ERAI_i}{H_{ER}} \quad (2)$$

$$MAPK_i = 1 - MAPKP_i \quad (3)$$

$$\frac{dMAPKP_i}{dt} = r_{ERAImapk} MAPK_i \Phi\left(ERAI_i, \kappa_{ERAImapk}, \nu_{ERAImapk}\right) - r_{LIPmapkp} MAPKP_i \Phi\left(LIP_i, \kappa_{LIPmapkp}, \nu_{LIPmapkp}\right) - \frac{MAPKP_i}{H_{MAPK}} \quad (4)$$

$$\frac{dNOTCH_i}{dt} = L_{NOTCH} - K_{DSLnotch} DSL_i NOTCH_i - K_{LAGnotch} NOTCH_i LAG_{adj(i)} - NOTCH_i\left[\frac{\Phi\left(MAPKP_i, \kappa_{MAPKPnotch}, \nu_{MAPKPnotch}\right)}{H_{NOTCHmn}} + \frac{1}{H_{NOTCH}}\right] \quad (5)$$

$$\frac{dNI}{dt} = K_{DSLnotch} DSL_i NOTCH_i + K_{LAGnotch} NOTCH_i LAG_{adj(i)} - \frac{NI_i}{H_{NOTCH}} \quad (6)$$

$$egf_{i \neq 4} = 0 \quad (7)$$

$$egf_4 = 1$$

$$\frac{dEGF_i}{dt} = L_{EGF} EGF_i + 2D_{EGF}\left(EGF_{adj(i)} - EGF_i\right) - EGF_i ER_i\left(\left(K_{EGFermx} - K_{EGFermn}\right)\Phi\left(MAPKP_i, \kappa_{MAPKPer}, \nu_{MAPKPer}\right) + K_{EGFermn}\right) - \frac{EGF_i}{H_{EGF}} \quad (8)$$

$$\frac{dLAG_i}{dt} = L_{LAG}\Phi\left(MAPKP_i, \kappa_{MAPKPlag}, \nu_{MAPKPlag}\right) - LAG_i NOTCH_{adj(i)} - \frac{LAG_i}{H_{LAG}} \quad (9)$$

$$\frac{dDSL_i}{dt} = L_{DSL}\Phi\left(MAPKP_i, \kappa_{MAPKPdsl}, \nu_{MAPKPdsl}\right) + 2D_{DSL}\left(DSL_{adj(i)} - DSL_i\right) - K_{DSLnotch} DSL_i NOTCH_i - \frac{DSL_i}{H_{DSL}} \quad (10)$$

$$\frac{dEGL_i}{dt} = L_{EGL}\Phi\left(MAPKP_i, \kappa_{MAPKPegl}, \nu_{MAPKPegl}\right) - \frac{EGL_i}{H_{EGL}} \quad (11)$$

$$\frac{dLIP_i}{dt} = L_{LIP}\Phi\left(NI_i, \kappa_{NIlip}, \nu_{NIlip}\right) - \frac{LIP_i}{H_{LIP}} \quad (12)$$

For inclusion of Notch-based degradation of LAG-2 (an alternative explored interaction), replace Equation 9 above with equation 13 below.

$$\frac{dLAG_i}{dt} = L_{LAG}\Phi\left(MAPKP_i\Psi\left(NOTCH_i, \kappa_{NOTCHlag}, \nu_{NOTCHlag}\right)\kappa_{MAPKPlag}, \nu_{MAPKPlag}\right) - LAG_i NOTCH_{adj(i)} - \frac{LAG_i}{H_{LAG}} \quad (13)$$

For models of an isolated VPC, we simulated a single cell with no LAG (deletion of equation 9 and LAG=0 for all time).

The notation for our parameters follows a fixed format, as follows:

Parameter Prefix	Description	Typical range
H_X	Mean lifetime of X	4-400
κ_{Xy}	Half-maximal activation coefficient (threshold) of X on target y	0.01-1
K_{Xy}	Rate of binding of receptor X with ligand y	0.01-1
ν_{Xy}	Hill coefficient of X on target y	1-8
r_{Xy}	Maximal rate of X on y	0.01-1
D_X	Diffusion/Transfer rate of X	0.0025-0.25
L_X	Synthesis rate of X	0.00025-2.5

The full list of model parameters and range explored in random search is shown below. The grey entries indicate parameters involved in an alternative explored network that tested the inhibition of LAG2 by Notch (equation 13).

Parameter	**Description**	**Range**	**Sampling**
H_{LAG}	Lifetime of LAG2	4-400	Log
H_{DSL}	Lifetime of DSL	4-400	Log
H_{EGF}	Lifetime of EGF	4-400	Log
H_{ER}	Lifetime of EGF receptor	4-400	Log
H_{MAPK}	Lifetime of MAPK	4-400	Log
H_{NOTCH}	Lifetime of Notch	4-400	Log
$H_{NOTCHmn}$	Lifetime of Notch when maximally degraded by MAPKP activity	1-H_{NOTCH}	Log
H_{LIP}	Lifetime of LIP1	4-400	Log
H_{EGL}	Lifetime of EGL17	4-400	Log
$\kappa_{ERAImapk}$	Threshold for ERAI activation of MAPK	0.01-1	Log
$\kappa_{LIPmapkp}$	Threshold for LIP1 inactivation of	0.01-1	Log

	MAPKP		
$\kappa_{MAPKPnotch}$	Threshold for MAPKP degradation of Notch	0.01-1	Log
$\kappa_{MAPKPer}$	Threshold for MAPKP increasing EGFR affinity for EGF (e.g. through EPS-8)	0.01-1	Log
$\kappa_{MAPKPegl}$	Threshold for MAPKP activation of EGL-17	0.01-1	Log
κ_{NIlip}	Threshold for NI activation of LIP1	0.01-1	Log
$\kappa_{MAPKPdsl}$	Threshold for MAPKP activation of DSL	0.01-1	Log
$\kappa_{NOTCHlag}$	Threshold for Notch inhibition of LAG2	0.01-1	Log
$r_{LIPmapk}$	Maximal rate of MAPKP dephosphorylation by LIP1	0.01-1	Log
$r_{ERAImapk}$	Maximal rate of MAPK phosphorylation by ERAI	0.01-1	Log
$K_{LAGnotch}$	Rate of binding of LAG2 to NOTCH	0.01-1	Log
$K_{DSLnotch}$	Rate of binding of DSL1 to NOTCH	0.01-1	Log
$K_{EGFermn}$	Basal rate of binding of EGF to EGFR (absence of EPS-8)	0.01-1	Log
$K_{EGFermx}$	Maximal rate of binding of EGF to EGFR (due to EPS-8)	$K_{EGFegfrmn}$ -1	Log
D_{EGF}	Fraction of EGF diffusing to neighboring cells	0.0025-0.25	Log
D_{DSL}	Fraction of EGF diffusing to neighboring cells	0.0025-0.25	Log
$v_{ERAImapk}$	Cooperativity of ERAI activation of MAPK	1-8	Integer
$v_{LIPmapkp}$	Cooperativity of LIP1 inactivation of MAPKP	1-8	Integer
$v_{MAPKPlag}$	Cooperativity of MAPKP activation of LAG2	1-8	Integer
$v_{MAPKPdsl}$	Cooperativity of MAPKP activation of DSL	1-8	Integer
$v_{MAPKPnotch}$	Cooperativity of MAPKP degradation of NOTCH	1-8	Integer
$v_{MAPKPer}$	Cooperativity of MAPKP increasing affinity for EGFR	1-8	Integer
v_{NIlip}	Cooperativity of NI in activating LIP1	1-8	Integer
$v_{MAPKPegl}$	Cooperativity of MAPKP activating EGL17	1-8	Integer
$v_{NOTCHlag}$	Cooperativity of NOTCH suppressing LAG2 synthesis	1-8	Integer
L_{EGF}	Synthesis rate for EGF	$\frac{1}{10\ H_{EGF}} - \frac{10}{H_{EGF}}$	Log
L_{LAG}	Synthesis rate for LAG-2	$\frac{1}{10\ H_{LAG2}} - \frac{10}{H_{LAG2}}$	Log

L_{DSL}	Synthesis rate for DSL	$\frac{1}{10\ H_{DSL}} - \frac{10}{H_{DSL}}$	Log
L_{NOTCH}	Synthesis rate for NOTCH	$\frac{1}{H_{NOTCH}}$	Fixed
L_{ER}	Synthesis rate for EGFR	$\frac{1}{H_{EGFR}}$	Fixed
L_{MAPK}	Synthesis rate for MAPK	$\frac{1}{H_{MAPK}}$	Fixed
L_{LIP}	Synthesis rate for LIP1	$\frac{1}{H_{LIP}}$	Fixed
L_{EGL}	Synthesis rate for EGL17	$\frac{1}{H_{EGL}}$	Fixed

Non-dimensionalization

We were interested in relative changes in protein levels, not the absolute concentrations. Synthesis rates (*L* parameters) changed only the scaling of the concentrations; these parameters could be constrained, allowing us to reduce the number of free parameters while still exploring the full dynamical behavior of the network. The synthesis rates were fixed at the reciprocal of the mean lifetimes for the random search. This restriction is equivalent to a non-dimensionalization scheme that normalizes the concentrations to their maximal steady state, as described previously (Meir et al., 2002a; Meir et al., 2002b; von Dassow et al., 2000). Thus, concentrations vary between 0 (no expression) and 1 (maximal). The concentrations of ER, MAPK, Lip1, Egl17, and Notch followed this scheme; EGF, LAG2, and DSL were allowed to vary over a larger range to allow for the possibility of stoichiometric differences between receptor and ligand (i.e. a molar excess of EGF over ER). Synthesis rates are present in the model (as opposed to completely removing them by non-dimensionalization) because they allowed us to easily simulate the effects of gene dosage changes.

Modeling software

Numerical integration and analysis used Mathematica version 5.2 (Wolfram Research). To test for errors in numerical integration, we compared a subset of the solutions generated by Mathematica to those from the gene network simulation software Ingeneue (Kim, 2009; Meir et al., 2002a). Ingeneue and Mathematica use different numerical integration schemes, and we found no difference between the solutions returned by the two programs. This network is available as a Mathematica notebook on request.

Simulation time and stability check

Cellular fate patterns were checked at 300 min. The exact number of tested parameter sets (close to 10^7) was arbitrary, but sufficient for us to reproduce lifelike behavior and make testable predictions about cell patterning and species differences. Patterns were considered stable if the cellular fates in all six cells did not change from 300 min to 400 min of simulated development, according to the criteria in Fig 1C. These times are arbitrary; altering these times slightly altered the fraction of parameter sets satisfying different conditions, but did not eliminate the ability of the

model to reproduce lifelike behavior. We enforced stability from 300 to 400 min to ensure reasonable stability over the relevant time window in developmental timing. A subset of our solutions do not maintain the wild-type pattern after 400 min, indicating that they have not reached a steady state, however, we assume that changes in expression long after vulva specification are unimportant. Thus, we did not require the system to be in steady state.

Bifurcation analysis for an isolated cell

The bifurcation diagrams were built using the software XPPAuto (Ermentrout, 2002), which calculated the steady-state of the system at the EGF concentration at which the isolated cell stably (checked at t=1000 min) adopted the 2° fate. The *egf* step size used to generate the bifurcation plots was 0.02.

Sequential induction versus Morphogen induction

Solutions that are "Morphogen induction sufficient" are those with a stable wild-type pattern that does not need Lag2 nor DSL diffusion. Solutions that are "Sequential sufficient" are those with a stable wild-type pattern that does not need EGFR expression nor EGF diffusion in P(5,7).p. These two manipulations are not fully equivalent because the concentration seen by P6.p differs. The first is closer to the *egfr* genetic mosaic experiments, while the second is most important to define the patterning mechanism. We therefore chose to perform both.

Statistical tests

The Kolmogorov-Smirnov tests of the significance of the difference between two parameter distributions were performed using the software R (www.R-project.org). For each patterning mode and for the species sets, the parameter distributions of solutions were compared against the distributions of all wild-type solutions (the reference distributions). Bonferroni corrections for the number of comparisons were implemented.

Classifying different species behaviors in the model

We searched for parameter sets that could reproduce the experimentally determined differences among *C. elegans*, *brenneri*, *remanei*, and *briggsae*. These species have the same wild-type pattern, but differences apear after *egf* overexpression or anhcor cell (AC) ablation. *egf* overexpression has been performed in *C. briggsae* and *C. elegans* only. To successfully reproduce a species behavior, a parameter set had to reproduce the wild type pattern and the pattern for AC ablation and *egf* overexpression (if known).

AC ablations: in these simulations, the initial *egf* mRNA concentration was 1 (wild-type), which was later reduced to 0 to simulate AC ablation. Ablations were performed every 10 min of simulation time (until t_{end}=300 min), which allowed us to uncover all (or most) possible intermediate patterns. The final molecular concentrations (at t_{end}) from a previous ablation were used as the initial conditions for the next ablation. This strategy allowed us to record a series of intermediate cell fate patterns from the 3°3°3°3°3°3° pattern (at very early ablations) to the wild-type (at late ablations). If any of these intermediates was 3°3°2°1°/2°2°3°, then the solution was considered to reproduce the *C. elegans* AC ablation behavior (Milloz et al., 2008). If any of these intermediates was 3°3°2°2°2°3° (3°3°2°3°2°3°), then the solution was considered to reproduce the *C. briggsae* (*C. remanei*) AC ablation behavior. In case of a direct transition from 3°3°3°3°3°3° to the wild-type pattern, the

solution was considered to reproduce the *C. brenneri* behavior (Félix, 2007). Our pattern requirements resulted in some overlap between *C. elegans* and *C. briggsae-like* solutions. This overlap results from P6.p becoming 1/2° using later ablation times in the *C. briggsae-like* solutions, and there is no experimental evidence showing that this may not be the case.

egf overexpressions were simulated by systematically increasing the initial *egf* mRNA levels using a geometric progression from 1.1 to 50, with common ratio of 1.1. The resulting cell fate pattern at each *egf* dose was determined at 300 min for each dose using the fate plane. We thus obtained a series of intermediate patterns from the wild-type (*egf* concentration of 1) to 1°1°1°1°1°1° (when *egf* levels were very high). If the first non wild-type pattern was 3°+2°1°2°+ (where "+" stands for an induced, non-3°, fate), then the solution was the *C. elegans egf* overexpression pattern (Table S6). If the first non wild-type pattern was 3°2°1°1°1°2°, then the solution was the *C. briggsae egf* overexpression pattern (Félix, 2007).

C. elegans N2-like solutions

The list of criteria that were used to classify solutions as "*C. elegans* N2-like" is indicated by stars in Table S7B.

Although the *lin-15* and *gap-1* genes were not explicitly included in the model, we simulated the *lin-15* and the *gap-1(0)* mutants by reproducing their known effects. LIN-15 is thought to act as by preventing ectopic activation of the EGF ligand in the surrounding epithelium, thus inhibiting excessive activation of the LET-23/EGFR pathway in the VPCs (Cui et al., 2006). We simulated this mutation by expressing the inductive signal in all VPCs. In *lin-15* defective animals, all VPCs assume vulval fates, with a normal 2°1°2° pattern for P5.p to P7.p, and some 1° fate induction in the other Pn.p cells or their daughters (Sternberg, 1988; Sternberg and Horvitz, 1989). We do not interpret the results as an alternation of 1° and 2° fates as are often schematically assumed.

GAP-1 is a direct inhibitor of the Ras protein (GTPase-activating protein), and a loss-of-function mutation in this gene has been shown to suppress the Vulvaless phenotype of mutations in the *let-60/Ras* pathway (Hajnal et al., 1997). The *gap-1(0)* mutation was simulated in the model by reducing the MAPK phosphorylation threshold, which increased Ras pathway sensitivity to the inductive signal. Different amounts of reduction in this threshold were tested for each solution, ranging from $1/\sqrt{2}$ of its original value to $1/(128*\sqrt{2})$. Changes in this threshold had to be silent, i.e. did not alter the wild-type pattern.

The *egfr(rf)* mutation was mimicked in the model by decreasing the initial EGFR concentration in all cells by some amount that caused a Vulvaless (or non wild-type) phenotype. Different initial EGFR concentrations were tested ranging from 0.7 to 0.01 (the same value was used for all cells).

We did not require the removal of the LIP-1 to MAPKP link to be silent (as is the actual *lip-1(0)* mutation; Berset et al., 2001) because other negative regulators of the Ras pathway downstream of Notch signaling are known and may produce mutant phenotypes in combination (Yoo et al., 2004).

We chose not to enforce further criteria to restrict the *C. elegans* N2 parameter space (Table S7B). The Notch knockout experimental result is unclear, as *lin-12* mutations affects anchor cell specification in addition to VPC specification (Greenwald et al., 1983). We also decided not to enforce the Isolated cell behavior because its implementation in the model imposed sharper boundaries between fates than was found in experiments (Katz et al., 1995).

Experimental Procedures

Strains

Strains were grown as previously described (Milloz et al., 2008) at 20°C, unless otherwise stated. In this experiment, the genetic background is N2. For laser ablations, we used as a wild-type either N2, or N2 carrying an *egl-17::CFP* reporter and a *lip-1::YFP* reporter (JU982, Milloz et al., 2008). As a *dsl-1(ok180null)* carrying strain we used GS3662 (Chen and Greenwald, 2004) or GS3662 carrying the *egl-17::CFP* reporter and a *lip-1::YFP* reporter (JU1215, this study). For the "genetic ablation" experiment, we used the strains CB1410 *unc-84(e1410)X* (Sternberg and Horvitz, 1986; Sulston and Horvitz, 1981) and JU1588 *dsl-1(ok180)IV unc-84(e1410)X* at 23°C (this study). In *unc-84(e1410)* worms grown at 23°C, most Pn cells (the mothers of Pn.p cells) failed to migrate to the ventral midline, except one (or two), resulting in a high frequency of worms with a single Pn.p cell (Sternberg and Horvitz, 1986).

For the *lin-3* doses in *C. elegans* N2 background, the following integrated transgenic lines were used. JU1072: *lin-3(e1417)*; *mfIs45[pJM1; unc-119(+); pmyo-2::DsRED2; pBS]*. JU1023: *mfIs44[pJM1; unc-119(+); pmyo-2::DsRED2; pBS]*. JU1024: *mfIs45[pJM1; unc-119(+); pmyo-2::DsRED2; pBS].* JU1105: *mfIs53[pRH9; unc-119(+); pmyo-2::DsRED2; pBS]*. JU957: *mfIs38[pJM1; unc-119(+); podr-1::DsRED; Cel genomic DNA].* JU1100: *mfIs51[pRH9; unc-119(+); pmyo-2::DsRED; pBS].*

For observation of *lip-1* reporters in *C. elegans* and *C. briggsae,* the following integrated transgenic lines were used. JU936: *mfIs29[Cel-lip-1::GFP, Cel-myo-2::GFP]* in *C. briggsae* AF16 background (Félix, 2007). AH142: *zhIs4[pTB10]III* (*Cel-lip-1::GFP* transcriptional reporter, Berset et al., 2001). JU982: *arIs92 V; mfIs41[pJM4; unc-119(+); Cel-myo-2::DsRED2]II* (pJM4 harbors the *Cel-lip-1::YFP* transcriptional reporter, Burdine et al., 1997; Milloz et al., 2008).

Genotyping of the *dsl-1* locus

To check for the presence of the *dsl-1(ok180)* allele for strain construction, we performed PCR on a mix of worms using a primer pair that flanked both side of the 2.2kbp deletion (GCCGAAAATTTTGGAGTTCA and ATCCAATTTTCCAGCCACAG) and with one primer flanking and one internal primer (GCCGAAAATTTTGGAGTTCA and ACGTATGCCACGAAGGATTC). Product size was checked by electrophoresis.

Pn.p cell ablation

To isolate a Pn.p cell from its neighbors, we ablated all the VPCs except one, before vulva induction, using a laser microbeam (Photonics Instruments) as described (Félix, 2007). The remaining VPCs tended to migrate towards the anchor cell.

In the *C. remanei-C. elegans* N2 experiments, all VPCs except P8.p were ablated. We selected worms from asynchronous 20°C cultures and staged them under Nomarski optics based on morphological traits and cell division pattern at the L1 lethargus to early L2 stage. We distinguished the lethargus L1 stage by the closed mouth and the size of the worm. The early L2 stage corresponds to the time between the molt and completion of the seam cell precursor division. The growth of the gonad was checked as an additional control. After ablation, worms were recovered and grown at 20°C.

In the genetic ablation experiment, we grew worms carrying the *unc-*

84(e1410ts)X mutation at 23°C (Sternberg and Horvitz, 1989). At this temperature, most Pn cells fail to migrate to the ventral midline and die, except one cell on average. We score the lineage in worms where a single Pn.p cell was found in the ventral midline.

In the experiment comparing *C. remanei* and *C. elegans*, P8.p was isolated rather than P4.p, because of the low vulval fate competence of P4.p in *C. remanei* (J.-B. P., unpublished results).

Cell lineage analysis

In the laser ablation experiment, the cell lineage was inferred from observations at the lethargus L3 stage and subsequent stages under Nomarski optics (100x objective), as described (Félix, 2007). Cell lineage nomenclature is given in Table S2. S or s are scored as 3° fates. LL, LL, and vulval sublineages with a cell adhering to the cuticle were scored as external 2°. TU was scored as an internal 2° fate and TT as a half 1°. O was interpreted as equivalent to a T. D was interpreted depending on the lineage context (for example, TDDT, 1°; LDTU, 2°). See Félix (2007) for discussion on ambiguous lineage cases.

In the genetic cell ablation experiment, we deduced the cell lineage by scoring the position and number of nuclei at the early L4 stage in worms where a single Pn.p has reached the ventral midline. In this case, we could accurately score the 1° and 2° fates, but less accurately 3° or fused fates due to difficulty in distinguishing between two cells resulting from the early fusion of two Pn.p cells to hyp7 (normally occurring for P1.p, P2.p, P9.p, P10.p and P11.p) and the two daughters produced by division of a 3° Pn.p. Thus, the outcome of the genetic ablation experiment is on the 1° and 2° cell fate only.

Construction of lines overexpressing *lin-3* from the anchor cell in *C. elegans*

Extra-chromosomal arrays were obtained by injecting a plasmid carrying a wild-type *lin-3(+)* region comprising only its anchor cell enhancer and promoter in front of the corresponding open reading frame (pRH9, Hill and Sternberg, 1992). pRH9 was injected at different concentrations with *unc-119(+)* plasmid, a fluorescent marker, and pBS-SK(+) plasmid (Addgene) or genomic DNA to bring the total DNA concentration to 100 ng/μL in H_2O.

For some lines, we used the *lin-3* gene with the *e1417* point mutation in the anchor cell enhancer that strongly reduces the anchor cell promoter activity (Hwang and Sternberg, 2004) (pJM1 plasmid). pJM1 contains the same 5.2 kbp *lin-3* region as pRH9 and was built by PCR amplification of the *lin-3* region (between the BamHI and HindIII restriction sites) in *lin-3(e1417)* mutant animals, using oligos CCGTGGATCCTTGAGCTTCTG and CAAGCTTGCCAACCCATTATC), which was then cloned in a pGEM-T Easy plasmid (Promega).

Injections were performed in the *unc-119(ed3)* background, and with the additional *lin-3(e1417)* mutation in the background for JU1072.

Stable genomic integration of the arrays was obtained after γ-ray irradiation and selection for non-Unc animals (Evans, 2006). The lines were backcrossed several times in the N2 background using the fluorescent markers. JU1024 was obtained by crossing the integrated transgene from JU1072 into the N2 background, thus removing the *lin-3(e1417)* mutation.

lip-1* expression in *C. briggsae* and *C. elegans

Animals between the L2 lethargus state and Pn.p division were mounted and

observed under a Zeiss AxioImager microscope as described (Milloz et al., 2008). Quantification data for *C. elegans* are those for *lip-1::YFP* in Milloz et al. (2008), using JU982. For comparison with the *C. briggsae* data, measurements were placed in three categories (integrated density over the nucleus: low<5,000; high>20,000).

Author Contributions

K.K. and E.H. wrote the code. E.H. produced the computational data for most figures. J.M., M.B., J.-B. P. and M.-A.F. performed experiments. M.-A.F., K.K., J.M., E.H. and E.M. designed the study. E.H., M.-A.F., K.K, J.M. and M.B. wrote the paper. M.-A.F., K.K. and E.M. supervised the work.

Supplemental References

Berset, T., Hoier, E. F., Battu, G., Canevascini, S., and Hajnal, A. (2001). Notch inhibition of RAS signaling through MAP kinase phosphatase LIP-1 during *C. elegans* vulval development. Science *291*, 1055-1058.

Berset, T. A., Hoier, E. F., and Hajnal, A. (2005). The *C. elegans* homolog of the mammalian tumor suppressor Dep-1/Scc1 inhibits EGFR signaling to regulate binary cell fate decisions. Genes Dev *19*, 1328-1340.

Burdine, R. D., Chen, E. B., Kwok, S. F., and Stern, M. J. (1997). *egl-17* encodes an invertebrate fibroblast growth factor family member required specifically for sex myoblast migration in *Caenorhabditis elegans*. Proc Nat Acad Sci USA *94*, 2433-2437.

Chen, N., and Greenwald, I. (2004). The lateral signal for LIN-12/Notch in *C. elegans* vulval development comprises redundant secreted and transmembrane DSL proteins. Dev Cell *6*, 183-192.

Clandinin, T. R., Katz, W. S., and Sternberg, P. W. (1997). *Caenorhabditis elegans* HOM-C genes regulate the response of vulval precursor cells to inductive signal. Dev Biol *182*, 150-161.

Cui, M., Chen, J., Myers, T. R., Hwang, B. J., Sternberg, P. W., Greenwald, I., and Han, M. (2006). SynMuv genes redundantly inhibit lin-3/EGF expression to prevent inappropriate vulval induction in *C. elegans*. Dev Cell *10*, 667-672.

Eisenmann, D. M., Maloof, J. N., Simske, J. S., Kenyon, C., and Kim, S. K. (1998). The β-catenin homolog BAR-1 and LET-60 Ras coordinately regulate the Hox gene *lin-39* during *Caenorhabditis elegans* vulval development. Development *125*, 3667-3680.

Ermentrout, B. (2002). Simulating, analyzing, and animating dynamical systems: a guide to XPPAUT for researchers and students (Philadelphia).

Evans, T. C. (2006). Transformation and microinjection. In Wormbook, The *C. elegans* Research Community, ed. (http://www.wormbook.org/). doi: 10.1895/wormbook.1.108.1.

Félix, M.-A. (2007). Cryptic quantitative evolution of the vulva intercellular signaling network in Caenorhabditis. Curr Biol *17*, 103-114.

Ferguson, E., and Horvitz, H. R. (1985). Identification and characterization of 22 genes that affect the vulval cell lineages of *Caenorhabditis elegans*. Genetics *110*, 17-72.

Greenwald, I. S., Sternberg, P. W., and Horvitz, H. R. (1983). The *lin-12* locus specifies cell fates in Caenorhabditis elegans. Cell *34*, 435-444.

Hajnal, A., Whitfield, C. W., and Kim, S. K. (1997). Inhibition of *Caenorhabditis elegans* vulval induction by *gap-1* and by *let-23* receptor tyrosine kinase. Genes Dev *11*, 2715-2728.

Hill, R. J., and Sternberg, P. W. (1992). The *lin-3* gene encodes an inductive signal for vulval development in *C. elegans*. Nature *358*, 470-476.

Hwang, B. J., and Sternberg, P. W. (2004). A cell-specific enhancer that specifies *lin-3* expression in the *C. elegans* anchor cell for vulval development. Development *131*, 143-151.

Inoue, T., Sherwood, D. R., Aspoeck, G., Butler, J. A., Gupta, B. P., Kirouac, M., Wang, M., Lee, P. Y., Kramer, J. M., Hope, I., et al. (2002). Gene expression markers for *Caenorhabditis elegans* vulval cells. Gene expression patterns *2*, 235-241.

Jacobsen, T. L., Brennan, K., Arias, A. M., and Muskavitch, M. A. (1998). Cis-interactions between Delta and Notch modulate neurogenic signalling in *Drosophila*. Development *125*, 4531-4540.

Katz, W. S., Hill, R. J., Clandinin, T. R., and Sternberg, P. W. (1995). Different levels of the *C. elegans* growth factor LIN-3 promote distinct vulval precursor fates. Cell *82*, 297-307.

Kim, K. J. (2009). Ingeneue: A software tool to simulate and explore genetic regulatory networks. In Methods in Molecular Biology, Systems Biology, I. V. Maly, ed. (Humana Press, Springer Science), pp. 169-200.

Koga, M., and Ohshima, Y. (1995). Mosaic analysis of the *let-23* gene function in vulval induction of *Caenorhabditis elegans.* Development *121*, 2655-2666.

Komatsu, H., Chao, M. Y., Larkins-Ford, J., Corkins, M. E., Somers, G. A., Tucey, T., Dionne, H. M., White, J. Q., Wani, K., Boxem, M., and Hart, A. C. (2008). OSM-11 facilitates LIN-12 Notch signaling during *Caenorhabditis elegans* vulval development. PLoS Biol *6*, e196.

Meir, E., Munro, E. M., Odell, G. M., and von Dassow, G. (2002a). Ingeneue: a versatile tool for reconstituting genetic networks, with example from the segment polarity network. J Exp Zool (Mol Dev Evol) *294*, 216-251.

Meir, E., von Dassow, G., Munro, E., and Odell, G. M. (2002b). Robustness, flexibility, and the role of lateral inhibition in the neurogenic network. Curr Biol *12*, 778-786.

Milloz, J., Duveau, F., Nuez, I., and Félix, M.-A. (2008). Intraspecific evolution of the intercellular signaling network underlying a robust developmental system. Genes Dev *22*, 3064-3075.

Shaye, D. D., and Greenwald, I. (2002). Endocytosis-mediated downregulation of LIN-12/Notch upon Ras activation in *Caenorhabditis elegans*. Nature *420*, 686-690.

Simske, J. S., and Kim, S. K. (1995). Sequential signalling during *Caenorhabditis elegans* vulval induction. Nature *375*, 142-146.

Sternberg, P. W. (1988). Lateral inhibition during vulval induction in *Caenorhabditis elegans*. Nature *335*, 551-554.

Sternberg, P. W. (2005). Vulval development. In Wormbook, The *C. elegans* Research Community, ed. (http://www.wormbook.org/). doi: 10.1895/wormbook.1891.1896.1891.

Sternberg, P. W., and Horvitz, H. R. (1986). Pattern formation during vulval development in *Caenorhabditis elegans*. Cell *44*, 761-772.

Sternberg, P. W., and Horvitz, H. R. (1989). The combined action of two intercellular signalling pathways specifies three cell fates during vulval induction in *C. elegans*. Cell *58*, 679-693.

Stetak, A., Hoier, E. F., Croce, A., Cassata, G., Di Fiore, P. P., and Hajnal, A. (2006). Cell fate-specific regulation of EGF receptor trafficking during *Caenorhabditis elegans* vulval development. EMBO J *25*, 2347-2357.

Sulston, J. E., and Horvitz, H. R. (1981). Abnormal cell lineages in mutants of the nematode *Caenorhabditis elegans*. Dev Biol *82*, 41-55.

Sundaram, M. V. (2005). The love-hate relationship between Ras and Notch. Genes Dev *19*, 1825-1839.

von Dassow, G., Meir, E., Munro, E. M., and Odell, G. M. (2000). The segment polarity network is a robust developmental module. Nature *406*, 188-192.

Yoo, A. S., Bais, C., and Greenwald, I. (2004). Crosstalk between the EGFR and LIN-12/Notch pathways in *C. elegans* vulval development. Science *303*, 663-666.